Potential of carbon dioxide transcritical power cycle waste-heat recovery systems for heavy-duty truck engines

Xiaoya Li[1,2], Hua Tian[1,*], Gequn Shu[1,*], Mingru Zhao[1], Christos N. Markides[2], Chen Hu[1]

[1] State Key Laboratory of Engines, Tianjin University, 92 Weijin Road, Nankai District, Tianjin 300072, China

[2] Clean Energy Processes (CEP) Laboratory, Department of Chemical Engineering, Imperial College London, UK

* Corresponding author. Tel: +86 22-27409558. E-mail: thtju@tju.edu.cn, sgq@tju.edu.cn

N.B.: This is the ACCEPTED MANUSCRIPT version of this article. The final, published version of the article can be found at: https://doi.org/10.1016/j.apenergy.2019.05.082

Abstract

Carbon dioxide transcritical power cycle (CTPC) systems are considered a new and particularly interesting technology for waste-heat recovery. In heavy-duty truck engine applications, challenges arise from the highly transient nature of the available heat sources. This paper presents an integrated model of CTPC systems recovering heat from a truck diesel engine, developed in GT-SUITE software and calibrated against experimental data, considers the likely fuel consumption improvements and identifies directions for further improvement. The transient performance of four different CTPC systems is predicted over a heavy-heavy duty driving cycle with a control structure comprising a mode switch module and two PID controllers implemented to realize stable, safe and optimal operation. Three operating modes are defined: startup mode, power mode, and stop mode. The results demonstrate that CTPC systems are robust and able to operate safely even when the heat sources are highly transient, indicating a promising potential for the deployment of this technology in such applications. Furthermore, a system layout with both a preheater and a recuperator appears as the most promising, allowing a 2.3% improvement in brake thermal efficiency over the whole driving cycle by utilizing 48.9% of the exhaust and 72.8% of the coolant energy, even when the pump and turbine efficiencies are as low as 50%. Finally, factor analysis suggests that important directions aimed at improving the performance and facilitating CTPC system integration with vehicle engines are: 1) ensuring long-duration operation in power mode, e.g., by employment in long-haul trucks; and 2) enhancing pump and turbine performance.

Keywords: carbon dioxide transcritical power cycle (CTPC); driving cycle; heavy-duty truck engine; integrated simulation; control structure; waste-heat recovery (WHR)

Nomenclature

A	flow area [m^2]	dc	driving cycle
A_s	heat transfer area [m^2]	eq	equivalent
c_p	specific heat capacity [J/(kg·K)]	exh	exhaust gas
K_P	pressure loss coefficient	f	working fluid
D	diameter [m]	g	saturated vapour
dx	discretization length [m]	gh	gas heater
e	total specific internal energy [J]; error	h	homogenous
E	parameter for Fr	in	inlet
f	friction factor	l	saturated liquid
F	parameter for Fr	p	pump
Fr	Froude number	pre	preheater
G	mass flux [kg/m^2·s]	r	relative
h	specific enthalpy [J/kg]	rec	recuperator
Δh	enthalpy change [J/kg]	t	turbine
H	parameter for Fr; total specific enthalpy [J/kg]	tp	two-phase
k	thermal conductivity [W/(m·K)]	th	thermal
m	mass of the volume [kg]	v	expansion valve
$\dot{m}$	mass flow rate [kg/s]	w	wall
L	length [m]		
N	engine speed [rpm, 1/s]	***Abbreviations***	
ΔP	pressure drop [Pa]	BMEP	brake mean effective pressure
P	pressure [Pa, MPa]	bsfc	brake specific fuel consumption
Pr	Prandtl number; pressure ratio	BTE	brake thermal efficiency
Q	heat exchanging quantity [W]	CAC	charge air cooler
R	radius [m]	CHP	cooling, heat and power
Re	Reynolds number	CO_2	carbon dioxide
t	time [s]	CTPC	carbon dioxide transcritical power cycle
T	temperature [ºC, K]; torque [N·m]	DE	diesel engine
u	fluid flow velocity [m/s]; controller input	ECU	electronic control unit

U	utilization rate	EGR	exhaust gas recirculation
V	vehicle speed [km/h, m/s]; volume flow rate [m^3/h]; volume [m^3]	ESC	European steady-state cycle
W	power [W]	Exp	experiment
We	Weber number	FRM	fast running model
x	vapour quality	HHDDT	heavy-heavy duty driving cycle
		IC	intercooler
Greek letters		ICE	internal combustion engine
α	heat transfer coefficient [W/(m^2·K)]	KNP	wirewound nonflame resistors
ρ	density [kg/m^3]	MP	modified pump
μ	viscosity [Pa·s]	MPC	model predictive control
η	efficiency	MT	modified turbine
ξ	time percentage	MPMT	modified pump and turbine
ω	speed [rpm, 1/s]	ORC	organic Rankine cycle
σ	surface tension [N/m]	OPOT	original pump and original turbine
γ	specific heat ratio	P-CTPC	preheated CTPC
		PR-CTPC	CTPC with recuperator and preheater
Subscripts		R-CTPC	regenerative CTPC
air	intake air	RC	Rankine cycle
c	condenser	sCO_2	supercritical CO_2
cl	coolant	Sim	simulation
cor	corrected	TDC	top dead centre
cw	cooling water	WHR	waste-heat recovery

1. Introduction

Current commercial heavy-duty diesel engines (DE) can achieve brake thermal efficiencies of up to about 40-45% [1], with the majority of the remaining thermal energy released by fuel combustion wasted in the form of exhaust gases expelled to the ambient and rejected via the engine coolant circuit, as summarized by Hoang [2] with reference to the heat wasted from typical diesel engines. Relevant waste-heat recovery (WHR) systems aim to capture this otherwise wasted energy and to convert this to usable power mechanically or electrically, thereby lowering the fuel consumption. The field of WHR from internal combustion engines has gained a substantial interest and attention from both industry and academia. Among all the popular WHR technologies such as turbo-compounding, thermoelectric generators and organic Rankine cycles (ORC), ORC technology stands out due to its overall performance, good thermal efficiency, flexible arrangements to fully extract energy from multiple heat sources, low cost and reduced backpressure impact on engine performance [3]. Therefore, in terms of energy savings and emission reductions, ORC technology is considered a promising solution in the context of WHR from both automotive and stationary engines [4] for secondary power generation.

1.1. Challenges in vehicle applications

Unlike stationary engine applications, for which mature and commercialized ORC systems have been developed and are in use, there are several prominent differences and challenges when it comes to on-highway vehicle applications especially long-haul trucks which have a large market share and present the greatest potential for engine WHR. Currently, ORC systems are still in a research and testing phase in this application. On the one hand, the available heat sources for recovery have transient and highly variable characteristics owing to the real-life operating profiles of engines under vehicle driving cycles. Agudelo et al. [5] evaluated the potential of exhaust energy from a diesel passenger car under European driving cycles and significant differences on the recovery potential were found at different points. These variable and transient heat sources lead to challenges for ORC system design and optimization. The performance of such systems at off-design conditions is of importance both overall, but also due to changes to the operational and performance characteristics of the pump, expander and heat exchangers. Chatzopoulou et al. [6] conducted off-design performance evaluations of ORC systems and reported results in which the ORC power was underestimated by up to 17% when component off-design performance was excluded. Shu et al. [7] compared the impact of the engine operating condition

selection on system design and concluded that a system designed under a partial engine condition can guarantee continuous operation within a broad range of conditions, and was therefore recommended for system design. Both Shu et al. [7] and Zhang et al. [8] developed predictive models of WHR systems and concluded that such systems are required to shut off at low-speed and low-torque engine conditions. Usman et al. [9] analysed the impacts of such systems on light duty vehicles and concluded that oversized heat exchangers bring difficulties in the maximum working fluid temperature control, while undersized ones sacrifice performance. Transient heat sources present further control challenges that need to be addressed to achieve good performance, reliability and durability, since accurate control strategies and robust controllers are required in these applications. Xie and Yang [10] simulated a Rankine cycle (RC) system under a driving cycle and reported that the operating mode switch can cause the on-road system efficiency to drop to 3.6%, which was less than half of the design value of 7.8%.

On the other hand, vehicle applications have additional and strict demands on installation space and weight. Battista et al. [11] evaluated the effects of an ORC WHR system for an engine in a light-duty vehicle application. Their results suggested that a weight increase causes an additional power demand equivalent to a loss of around 1% in fuel economy. Therefore, smaller-scale ORC systems might have a better potential of commercialization. These requirements call for safe working fluids, simple layouts and compact components, and at the same time high utilization rate realization of any alternative heat sources that also have different quantities (amount of energy available) and qualities (exergy due to the different temperature levels, thermal inertia and the influence on engine).

Over the past decades, great emphasis has been placed on bottoming ORC technologies for long-haul trucks. Cutting-edge RC/ORC technology developments from leading companies in this area are summarized in Appendix A. Nevertheless, and despite the significant R&D that has been performed in this field to-date, no ideal working fluid, cycle and system configuration/layout have been identified for on-highway heavy-duty engines. Although water [14], ethanol [15] and R245fa [17] are recognized as suitable fluids, they can only make use of waste-heat from the exhaust and/or EGR. The simultaneous recovery of thermal energy from both high-temperature and low-temperature heat sources requires dual-loop layouts which lead to bulky and heavy WHR systems [22]. Furthermore, organic working fluids cannot be directly heated to very high temperatures due to their relatively low thermal decomposition temperatures [23,24]. Next-generation working fluids and system layouts appear as key areas of further research and development for future commercialization for truck applications.

1.2. State-of-art of CO_2 as a working fluid

Carbon dioxide (CO_2) is a natural and environmentally-friendly working fluid that has appeared, amongst other, as an alternative to organic working fluids in automobile WHR applications. In 2005, Chen et al. [25] originally proposed a CO_2 bottoming system for WHR in vehicles to reduce fuel consumption. They compared three different types of cycles: a CO_2 transcritical power cycle (CTPC), a (supercritical) CO_2 Brayton cycle and a CO_2 cycle combining an air-conditioning cycle and a Brayton cycle. Based on the comparison of operating pressures, performance and optimization potential, the CTPC was deemed more attractive than the others and recommended for vehicle applications. Later, the authors compared a CTPC with an ORC system using R123 [26] and results indicated that the former obtained a slightly higher useful power-to-weight ratio (8.16 kW/kg for the CTPC compared to 8.06 kW/kg for the ORC) when utilizing the same heat source. Since then, CTPC-based systems have featured in many studies focused on vehicle WHR.

The working principle of the CTPC is similar to that of the ORC, only replacing the organic working fluid with CO_2. However, the CTPC has some notable advantages. Firstly, it can achieve a better thermal match to the heat sources thanks to the supercritical temperature glide of CO_2 [26,27], meanwhile CO_2 can be heated to high temperatures without decomposition concerns [28] due to its good thermal stability. Furthermore, the CTPC promises miniaturization, which can lead to system size reduction and ease of installation. Compact components can be adopted due to the high density and low viscosity of supercritical CO_2 (sCO_2). Persichilli et al. [29] demonstrated that CO_2 power cycle can feature an extremely compact turbine and also smaller microchannel heat exchangers than those used in RC systems. Shu et al. [30] considered the heat exchanger areas and turbine sizes for a CTPC system and an ORC systems using R123 as the working fluid, and suggested that the use of smaller flow channels and turbine sizes that can be accommodated by the former can give rise to some benefits in terms of size. Moreover, CTPC systems can extract energy from the engine coolant and exhaust-gas streams simultaneously thanks to its specific heat capacity properties [31]. An ideal turbine inlet temperature was found for which the CTPC system can make full use of both the thermal energy recovered by the engine coolant and exhaust streams [31]. Despite some challenges, such the need for high operating pressures relative to RC/ORC systems that lead added costs and safety concerns, and the low condensing temperatures that make it difficult to identify suitable heat sinks especially in mobile applications, CTPC WHR systems continue to present a serious challenge to

conventional RC/ORC technology with significant fundamental and practical interest.

Studies of engine WHR using CO_2 as the working fluid have been conducted both theoretically and experimentally. Farzaneh-Gord et al. [32] considered a CTPC system extracting energy from a natural-gas fired engine and its feasibility was demonstrated through thermodynamic modelling. Shu et al. [33] provided three comprehensive selection maps based on net power output, exergy efficiency and cost analysis. Similarly, Wu et al. [34] performed system optimization by using a genetic algorithm aiming to achieve the best power output and different layouts were recommended for heat sources with diverse characteristics. Li et al. [35] paid special attention to the dynamic performance of CTPC systems. Dynamic responses were modelled by using a predictive model and the sensitivity analysis identified the mass flow rate of the working fluid as the parameter with the greatest impact on system performance. This knowledge provides invaluable guidance in the design of CTPC systems.

Farouk and Hasan [36] considered component design and examined numerically the thermal transport characteristics of sCO_2, while Wang et al. [37] proposed an open-cell metal foam wrapped tube structure for heat transfer enhancement in exhaust heat exchangers and concluded, following numerical modelling, that it was associated with a more than ten-fold improvement relative to a bare-structure heat exchangers. Qi et al. [38] explored the design performance of sCO_2 radial turbines in the 100-200 kW range. The consideration of geometric features, operating constraints and loss mechanisms provided new insight towards the design of small-scale sCO_2 turbines. Experimentally, Shi et al. [39] established a CTPC system test-bench using an expansion valve for WHR from a DE. Tests were conducted with four different system layouts to compare their thermodynamic performance, however, due to the lack of a real expansion machine the net power output and thermal efficiency were estimated. Following this work, Li et al. [40-42] focused on the dynamic behaviour of such systems, by generating detailed test-data with respect to key variable perturbations. Such results promote a much better understanding of the open-loop dynamic behaviour of these systems, although active control strategies also require careful examination. Finally, Ge et al. [43] studied experimentally a CTPC system with a single-stage axial CO_2 turbine rated at 5 kW for WHR from an 80 kW micro-turbine CHP unit, while Pan et al. [44] established a CTPC test-rig using an electric heater and specifically focused on the design and testing of a 2 kW rolling piston expander, with the heat source (thermal oil) temperature kept below 200 ºC, which is different from the conditions expected in engine exhaust-gas streams.

1.3. Aims of the current work

Even though CTPC systems have gained some attention as a next-generation WHR technology, their technical and commercial viability is as yet unproven. Typically, simulations and experimental efforts are conducted separately, with insights reported in separate publications, while model calibration of individual components is often not available. Aspects such as system performance in actual scenarios, limiting factors or directions for further improvement are not considered in detail. The potential of CTPC systems in vehicle applications with highly transient heat sources remains unclear.

Therefore and in order to eliminate the gap between tests on a laboratory test facilities and actual expected performance in a real application, an integrated model of a target truck, engine and CTPC systems is developed in the GT-SUITE software environment and carefully calibrated against experimental data. After calibration, the simulation models are regarded as virtual test benches suitable for predicting the transient performance of CTPC systems over a cruise driving cycle, and studying the likely fuel consumption in real applications. Four different CTPC system layouts are examined including a basic CTPC, a regenerative CTPC (R-CTPC), a preheated CTPC (P-CTPC) and a CTPC with both a recuperator and a preheater (PR-CTPC). A control structure comprising a mode switch module and two PID controllers is proposed for stable, safe and optimal operation. Moreover, a detailed analysis of further improvements and of the ultimate potential of this technology after further system optimization is performed with a view towards real applications, in order to identify further improvement directions, as well as demonstrate the potential of the technology.

This paper is organized as follows: Section 2 describes the system modelling and calibration mainly including the DE and the CTPC systems. Section 3 presents the control strategies of CTPC systems together with performance prediction over a cruise driving cycle of heavy-heavy duty driving cycle (HHDDT). In Section 4, optimization potential is comprehensively provided through factor analysis. The paper ends with the main conclusions in Section 5.

2. System modelling

Figure 1 shows an integrated model of the whole system considered in this work, which consists of the truck, its transmission system and diesel engine, the CTPC system and driver. In this paper, CTPC systems are used to recover waste heat from a heavy-duty DE. The engine, YC6L330, is made by the Guangxi Yuchai Machinery Group. It is a typical inline, 4-stroke, 6-cylinder water-cooled

turbo-charged engine, with a bore of 113 mm, a stroke of 140 mm, and a displacement of 8.424 L as stated in manufacturer datasheet. The engine's rated power is 243 kW and its rated speed is 2200 rpm. This type of engine is widely used on long-haul heavy trucks such as the one targeted in current study (LZ3312H5FB). The truck has a Faster 10JSD140B gearbox and 12 tires with the type of Bridgestone M858SUPER (11.00R20), with the curb weight of 14.78 tons and the load capacity of 16.03 tons. Since we do not pay much attention to the models of the tractor, trailer, transmission, driver and ECU, these models and corresponding parameters are not specified here to avoid redundancy.

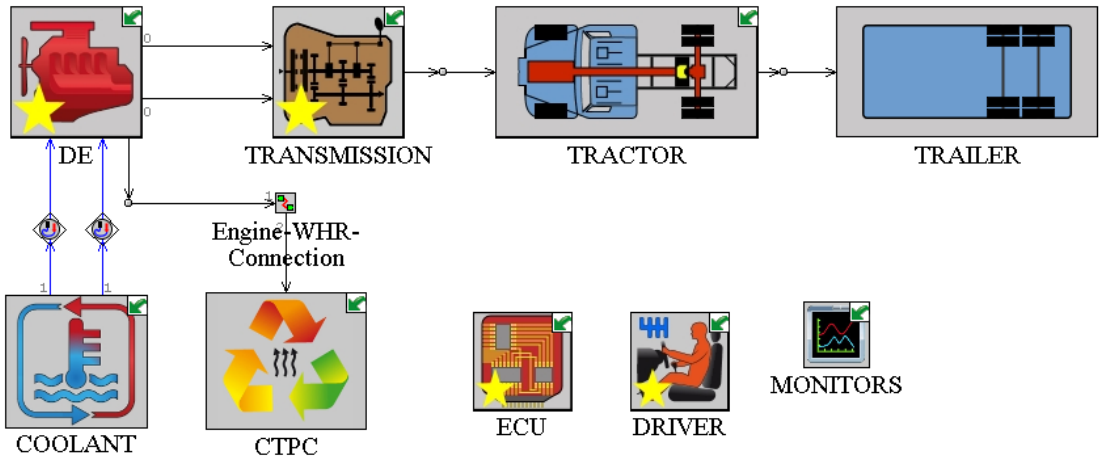


Fig. 1. Integrated model of the truck, transmission system, diesel engine, CTPC system and driver.

2.1. Diesel engine modelling

The engine modelling process involves two stages in this research. In the first stage, a detailed, high-fidelity engine model is built and calibrated against experimental data. Following this stage, the detailed model is simplified and converted into a fast running model (FRM) in order to reduce the simulation time. Furthermore, in this second stage, results from the FRM of the DE are compared to experimental data as well as simulation results from the detailed model as means of demonstrating reasonable accuracy and runtime. The FRM lumps various flow volumes together and allows for a large time-step size. It is much more attractive for engine incorporation into system level models where long transient events may be simulated such as waste-heat recovery and vehicle thermal management. Therefore, numerous sub-volumes in the exhaust manifold, exhaust pipes, intake manifold, compressor outlet pipes and intake pipes are lumped separately to reduce the total number of volumes. Figure 2 shows the final FRM of the engine as developed in this work.

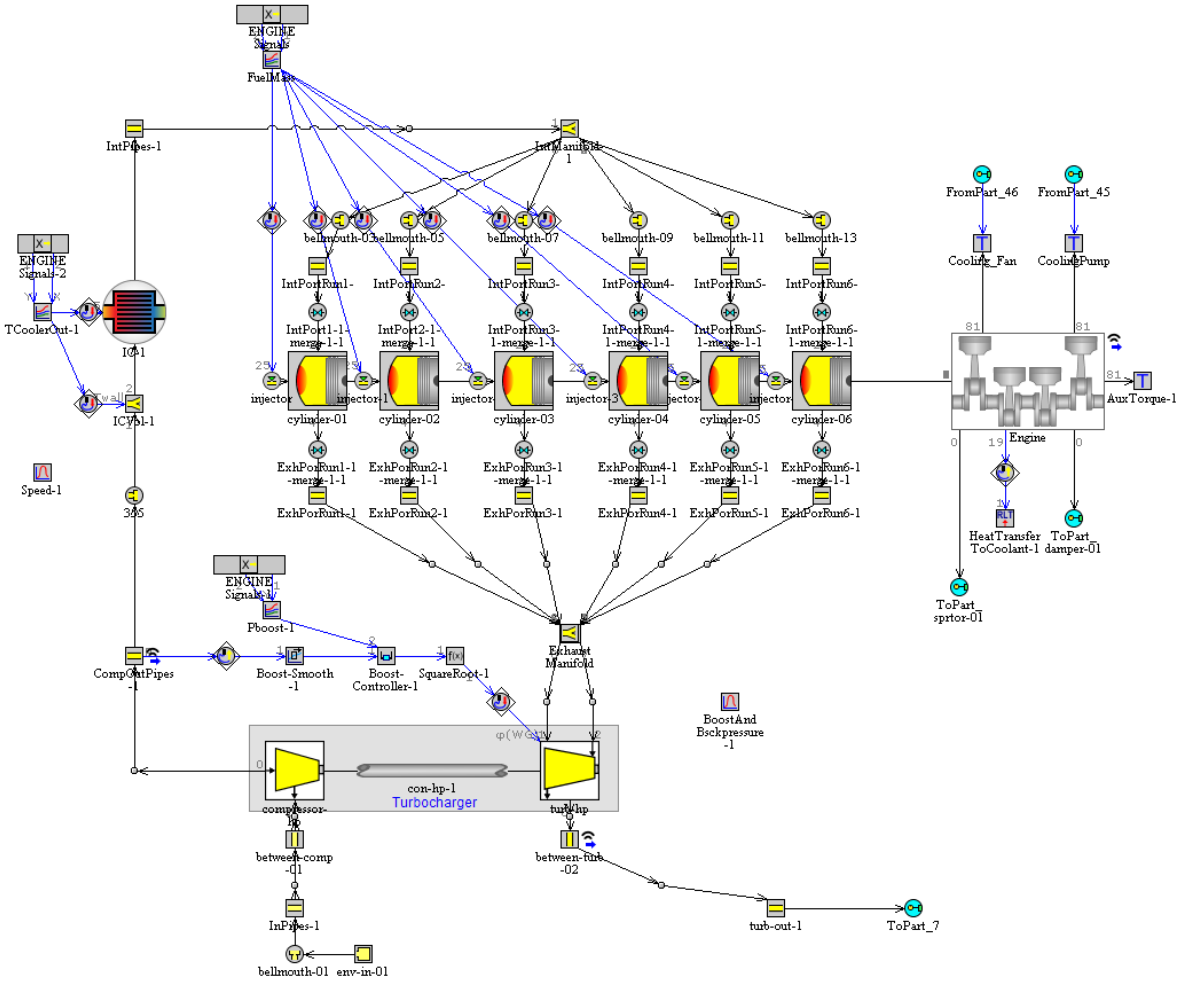


Fig. 2. Fast running model of diesel engine.

2.1.1. Model definition

The engine model contains the intake and exhaust pipes and valves, injectors, cylinders, crankshaft, turbocharger and intercooler (IC). It is built by a 1-D simulation software GT-SUITE (version 2016), which is widely used in vehicle industry. The primary data of these models include geometric parameters, performance profiles and simulation methods. Table 1 lists the main parameters of the diesel engine considered in this work. Additional parameters are described below.

The models of intake and exhaust pipes are firstly built based on the measured geometric data to reflect the real pipes therefore many sub-pipes such as bends, small pipes and flow-split pipes exist on the map. To achieve a fast running, these sub-pipes are lumped reasonably and only two volumes left for each cylinder to represent the intake ducting and exhaust ducting respectively.

Injectors are the key part in fuel supply system. Except the geometry of the nozzle, there are two more main parameters including injected mass and injection timing. They are obtained from the manufacturer and experiments. Injection rate maps against different engine speed and engine load are inputted to the injectors, and an injected fuel mass map against different engine speed and engine load is used to realize a map-based control of the requested fuel mass.

In the cylinders, the combustion and heat transfer models are important in maintaining a good prediction accuracy. Here, the classical Woschni correlation without swirl is used to calculate the in-cylinder heat transfer since the measured swirl data are not available. Combustion is modelled with cumulative heat release profiles, which is obtained by in-cylinder pressure measurements from the test bench. In cylinder chamber, two temperature zones method is used to calculate independently for the burned and unburned gases. The model of the engine crankshaft used in the present work contains a Chen-Flynn engine friction model, a 100% load table (the maximum BMEP curve) and the firing order. Data are obtained from the manufactures and experiments.

Turbocharger contains a turbine, a compressor and the coaxial high-speed shaft. The simulation is conducted based on their performance map, provided by the manufactures. A PID controller is used to control the boost pressure according to the engine conditions through waste gate diameter adjustment.

As for the intercooler, it is originally modelled by a bundle of pipes and then replaced with a FlowSplit template to represent the intercooler core. In this way, a HeatExchangerConn template is added to assure the intercooler outlet temperature is maintained. The diameter for this connection is calibrated. In addition, a 2-D lookup map of intercooler outlet temperature is implemented to match the test data and engine requirement at different engine conditions.

Table 1. Main parameters of diesel engine.

	Parameters	**Unit**	**Value**
Cylinder geometry	Bore	mm	113
	Stroke	mm	140
	Connecting rod length	mm	209.4
	TDC clearance height	mm	0.8
	Wrist pin to crank offset	mm	1
Piston cup geometry	Maximum diameter	mm	80
	Depth at maximum diameter	mm	22

	Centre depth	mm	7.3
Injector geometry	Nozzle hole diameter	mm	0.167
	Number of holes per nozzle	-	8
Valves geometry	Intake valve lash	mm	0.4
	Intake valve diameter	mm	34.3
	Exhaust valve lash	mm	0.45
	Exhaust valve diameter	mm	32.3
Heat transfer	Head temperature	K	590
	Piston temperature	K	600
	Cylinder temperature	K	480
	Cylinder heat transfer model	-	Woschni
Crankshaft	Firing order	-	1-5-3-6-2-4
	Effective rotating inertia	kg-m^2	2.5

2.1.2. Model calibration

Since the engine operates under a mapping condition, only several typical operating conditions are chosen for model calibration. Six conditions at full load are selected where engine speed is from 1200 rpm to 2200 rpm with an interval of 200 rpm. All experimental data are taken from the heat-balance tests [24] performed on the studied diesel engine, which are detailed in Ref. [45] and Ref. [46].

Figure 3 demonstrates the relative errors between the FRM simulation and experimental data as well as the detailed model simulation. Detailed information (data) relating to the calculation of the relative errors in Figure 3 is provided in Appendix B. Comparison has been conducted for nine representative parameters including brake specific fuel consumption (bsfc), engine power (W_{ICE}), engine torque (T_{ICE}), mass flow rate of intake air (m_{air}) and exhaust (m_{exh}), pressure at the inlet ($P_{IC,in}$) and outlet ($P_{IC,out}$) of the intercooler, temperature at the outlet of the intercooler ($T_{IC,in}$) and exhaust temperature (T_{exh}). From Figure 3, we observe that the maximum relative error between the FRM simulation and experimental data occurs in T_{exh} with the value of 9.2% while the largest relative error, 5.5%, appears in m_{air} between the FRM simulation and the detailed model. The discrepancy is caused by the differences between the combustion models and the real combustion processes. All relative errors are smaller than 10%, which is considered here adequate for early-stage engineering estimates, indicating a high accuracy simulation model that can be used for performance predictions. Therefore,

the DE FRM can be used reliably to generate representative transient heat sources over a cruise driving cycle of interest to the present study.

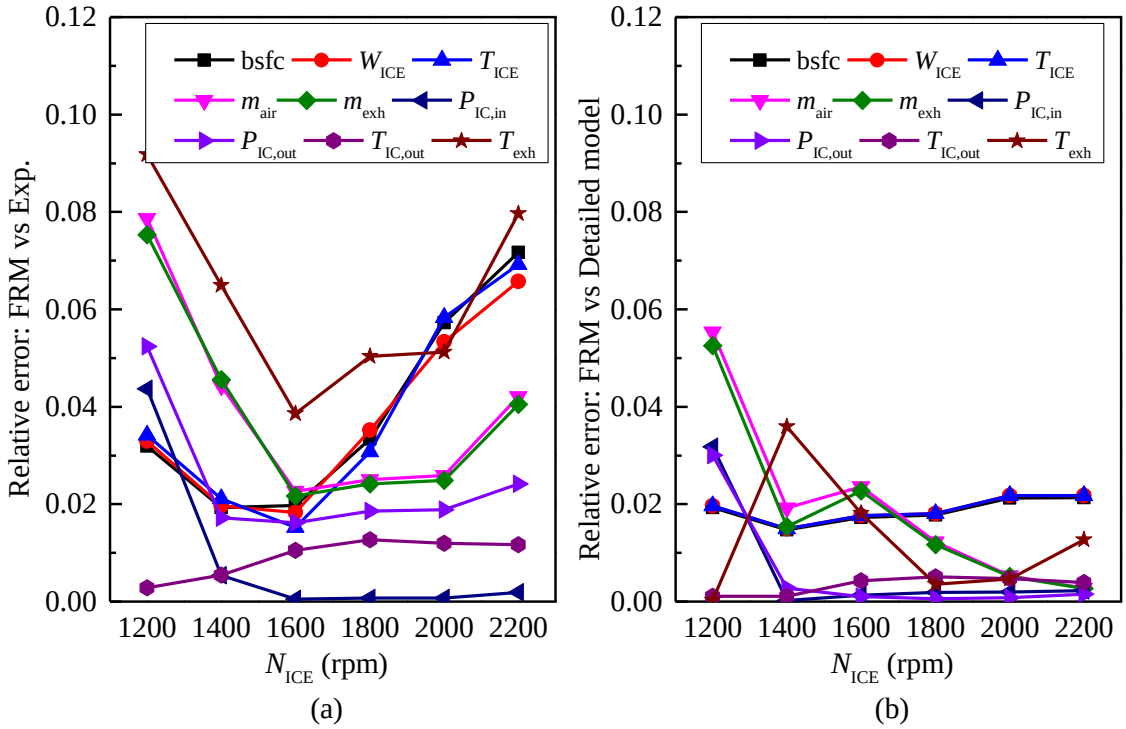


Fig. 3. ICE model calibration: relative error of (a) FRM simulation vs. experimental data; (b) FRM simulation vs detailed model simulation.

2.2. CTPC system modelling

CTPC systems considered here include four different layouts: a basic CTPC system to recover exhaust energy only, a regenerative CTPC (R-CTPC) to further extract the energy after the turbine, a CTPC with a preheater (P-CTPC) to extract engine coolant and exhaust energy, and a regenerative CTPC with a preheater (PR-CTPC) to fully use the energy of exhaust, coolant and after-turbine energy. PR-CTPC is taken as an example for the analysis below.

2.2.1. Model definition

The PR-CTPC system mainly contains a gas heater, a preheater, a recuperator, a condenser, a pump, a turbine and a receiver. The models are also built in GT-SUITE (version 2016), with Refprop 9.1 to calculate fluid properties. Figure 4 shows the final view of the PR-CTPC system.

To reproduce the behaviour of the real components, two categories of data are required for modelling and calibration in GT-SUITE: test data and geometric data. For any type of heat exchanger, test data are required for each fluid: inlet conditions (pressure, temperature or quality), outlet conditions (temperature and pressure), flow rate and heat transfer rate. For pump or turbine, detailed models are recommended to represent the real ones. Test data are used to create their performance maps.

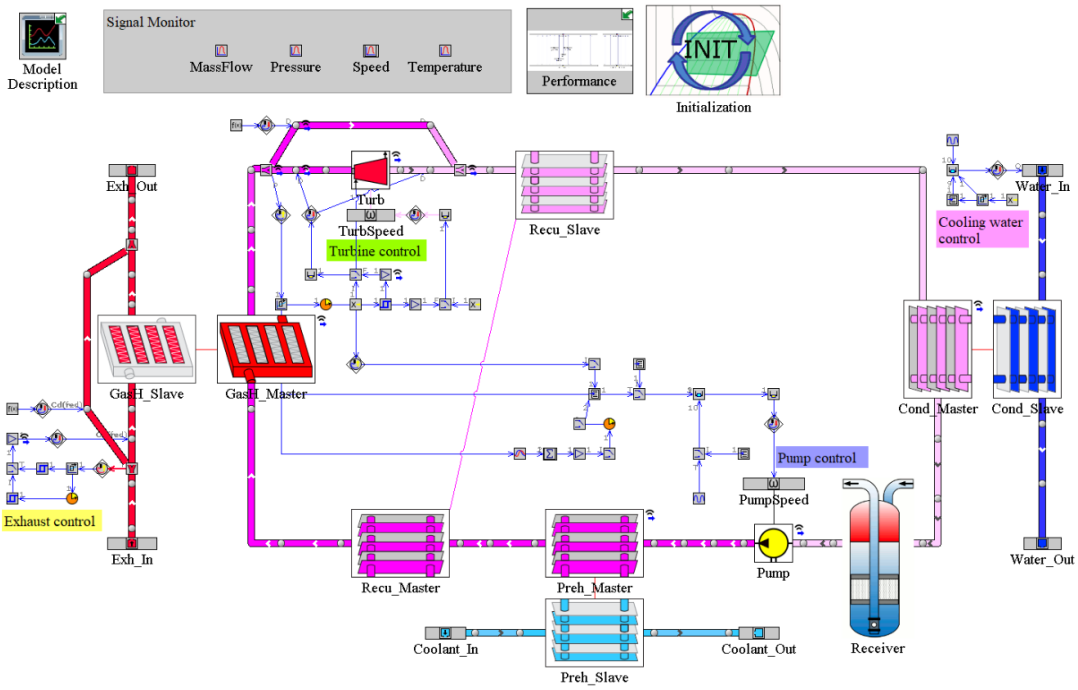


Fig. 4. CTPC model (example of PR-CTPC system).

(1) Gas heater model:

The gas heater is a self-designed heat exchanger, which is of tube-in-tube type. Figure 5 demonstrates the structure of the gas heater using in our test bench [47]. Since it is the first trial to apply CTPC systems to engine waste-heat recovery and the back pressure increased by the gas heater would deteriorate engine performance, the simplest tube-in-tube type is chosen. Exhaust gas travels through the outer tubes while CO_2 flows in the inner tubes. There are two outer tubes parallel to each other. Three identical inner tubes are arranged in each outer tube. Since there is no standard model in GT-SUITE, a general geometry model is applied through the template of "HxGeomGeneral". Reference length, heat transfer area, flow area and connection diameters are from the designed parameter as listed in Table 2 and further calculation.

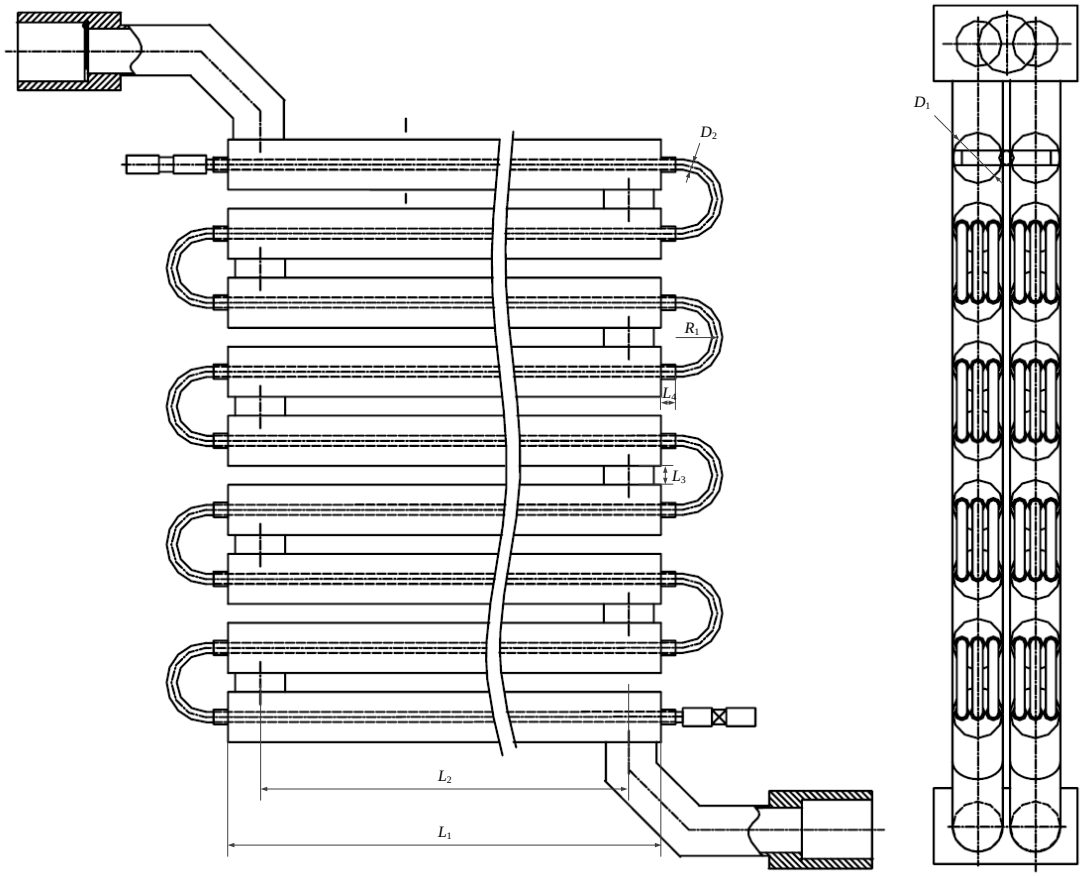


Fig. 5. Structure of the gas heater.

In the gas heater, both the exhaust and CO_2 flow as single-phase fluids. Therefore, typical heat transfer correlation, the Dittus-Boelter correlation [48] as shown in Eq. (1), is selected to calculate the heat transfer coefficients in the gas heater. A heat transfer map based on the experimental data is used to modify the calculation of supercritical heat transfer multiplier.

$$\begin{aligned} \alpha &= 0.023 \cdot \mathrm{Re}^{0.8} \cdot \mathrm{Pr}^{0.4} \cdot \frac{k}{D_{\mathrm{eq}}} \ \text{(heating)} \\ \alpha &= 0.023 \cdot \mathrm{Re}^{0.8} \cdot \mathrm{Pr}^{0.3} \cdot \frac{k}{D_{\mathrm{eq}}} \ \text{(cooling)} \end{aligned} \tag{1}$$

For the calculation of pressure losses, a pressure loss coefficient (K_P) is firstly calibrated from the experimental data through a simulation pre-processing routine. The measured pressure drop and flow rate data are used to perform an optimization aimed at finding an orifice discharge coefficient in each flow direction and a pipe friction multiplier that minimizes the errors between predicted and measured pressure drops over all of the entered data points. These are then applied in the ensuing simulation as physical representations of the restriction of the heat exchanger, and assumed to be constant. It is

worth noticing that the measured data are only used within the pre-processing optimization routine. Therefore, the pressure losses are simulated as follows [48]:

$$\Delta P = \frac{1}{2} \cdot \rho \cdot u^2 \cdot K_{\mathrm{p}} \tag{2}$$

$$u = \frac{\dot{m}}{\rho \cdot A_{\mathrm{eq}}} \tag{3}$$

where ρ is the fluid density, u is the fluid flow velocity; A_{eq} is the equivalent flow area; and $\dot{m}$ is the mass flow rate.

(2) Other heat exchanger model (plate type):

Except the gas heater, all the other heat exchangers are off-the-shelf which are of brazed-plate type. Table 2 lists their geometric parameters. "HxGeomPlate" template is used to build the geometry. All models require the experimental data of heat transfer and pressure drop for the calibration of heat transfer multipliers and pressure loss coefficients. In the recuperator, a two-sided Nusselt-Reynolds correlation is selected to calibrate this heat-exchange component.

For heat transfer calculation, the Dittus-Boelter correlation [48] is still adopted for the single-phase zone. However, the Yan-Lio-Lin correlation [49], shown in Eq. (4), is chosen for the two-phase zone as it provides a reasonably accurate prediction for plate condensation:

$$\alpha = 4.118 \cdot \mathrm{Re}_{\mathrm{eq}}{}^{0.4} \cdot \mathrm{Pr}_{\mathrm{l}}^{1/3} \cdot \frac{k_{\mathrm{l}}}{D_{\mathrm{eq}}} \tag{4}$$

$$\mathrm{Re}_{\mathrm{eq}} = \frac{G \cdot \left(1 - x + x\sqrt{\rho_{\mathrm{l}} / \rho_{\mathrm{g}}}\right) D_{\mathrm{eq}}}{\mu_{\mathrm{l}}} \tag{5}$$

$$\mathrm{Pr}_{\mathrm{l}} = \frac{c_{\mathrm{p}} \cdot \mu_{\mathrm{l}}}{k_{\mathrm{l}}} \tag{6}$$

where Re is the Reynolds number; Pr is the Prandtl number; k is the fluid thermal conductivity; D_{eq} is the equivalent diameter; G is the mass flux; x is the fluid quality; μ is the viscosity; c_{p} is the specific heat capacity; and subscripts l and g refer to liquid phase and vapour phase, respectively.

For pressure drop calculations, the same method expressed by Eq. (2) and Eq. (3) is applied for the single-phase zone, while for the two-phase zone (condensation), the Friedel friction correlation [50]

is used to produce a multiplier to adjust energy and momentum transfer. The two-phase pressure drop is therefore obtained by adjusting the liquid-phase pressure drop, which can be described as:

$$\Delta P_{tp} = \Delta P_l \cdot \left(E + \frac{3.24 \cdot F \cdot H}{Fr^{0.045} \cdot We^{0.035}} \right) \tag{7}$$

$$Fr = \frac{G^2}{g \cdot D_{eq} \cdot \rho_h{}^2} \tag{8}$$

$$We = \frac{G^2 \cdot D_{eq}}{\sigma \cdot \rho_h} \tag{9}$$

$$E = (1-x)^2 + x^2 \cdot \frac{\rho_l \cdot f_g}{\rho_g \cdot f_l} \tag{10}$$

$$F = x^{0.78} \cdot (1-x)^{0.224} \tag{11}$$

$$H = \left(\frac{\rho_l}{\rho_g} \right)^{0.91} \cdot \left(\frac{\mu_g}{\mu_l} \right)^{0.19} \cdot \left(1 - \frac{\mu_g}{\mu_l} \right)^{0.7} \tag{12}$$

$$F = x^{0.78} \cdot (1-x)^{0.224} \tag{13}$$

$$\rho_h = \left(\frac{x}{\rho_g} + \frac{1-x}{\rho_l} \right)^{-1} \tag{14}$$

wherein, *Fr* refers to Froude number; *We* means Weber number; σ is surface tension; ρ_h is homogenous density. Others are the same as described above.

Table 2. Geometric parameters of the heat exchangers.

Heat exchanger	**Parameters**	**Unit**	**Value**
Gas heater	Outer tube diameter (D_1)	mm	69
	Inner tube diameter (D_2)	mm	14
	Outer tube length per row (L_1)	mm	1303
	Outer tube connection distance (L_2)	mm	1214
	Outer tube connection height (L_3)	mm	26
	Inner tube port length (L_4)	mm	30
	Inner tube connection bend radius (R_1)	mm	47.5
	Wall thickness	mm	2
	Material	-	copper
Plate heat exchangers	Plate length	mm	377
	Plate width	mm	119.5

	Channel volume	dm^3	0.061
	Channel plate material	-	stainless steel
Recuperator	Connection port diameter	mm	18
	Number of plate	-	40
	Total weight	kg	14
Preheater	Connection port diameter	mm	24
	Number of plate	-	40
	Total weight	kg	14
Condenser	Connection port diameter	mm	24
	Number of plate	-	80
	Total weight	kg	24

(3) Pump and turbine model:

A three-piston reciprocating plunger pump is installed and applied here. The displacement is 1.7 m^3/h and the maximum speed is 167 rpm. A series of tests was performed under different conditions. Therefore a "PumpMap" template is used to calibrate the pump. Totally, 102 sets of data from 30 rpm to 150 rpm are filled in. The data for each speed line consist of several sets of volumetric flow rate, pressure rise and efficiency. Therefore, each speed line could be fitted thus creating the pump map. Figure 6 shows the pump map at different speeds, with all data coming from tests. It should be noted that for safety, pump outlet pressure is lower than 11 MPa during experiments therefore the maximum pressure rise is less than 6 MPa. Moreover, a safety threshold is considered so the pump speed is limited to 150 rpm. After the pre-processing step, an extrapolated performance map that contains 3600 operating points (60 speeds x 60 pressure ratios) is generated according to the pump affinity laws and interpolation logic. During the simulation process, the inputs to the solution at each time step are the shaft speed and the pressure rise across the pump. The solver looks for the mass flow rate and efficiency for that speed and pressure ratio based on the pre-process pump map. The outlet enthalpy and compression power are calculated from:

$$h_{\mathrm{p,out}} = h_{\mathrm{p,in}} + \Delta h_{\mathrm{s,p}} / \eta_{\mathrm{p}} \tag{15}$$

$$W_{\mathrm{p}} = \dot{m}_{\mathrm{f}} \cdot \left(h_{\mathrm{p,out}} - h_{\mathrm{p,in}} \right) \tag{16}$$

$$\Delta h_{\mathrm{s,p}} = \left(P_{\mathrm{p,out}} - P_{\mathrm{p,in}} \right) / \rho_{\mathrm{p,in}} \tag{17}$$

where $h_{p,out}$ and $h_{p,in}$ represent the specific enthalpy at the outlet and inlet of the pump; $P_{p,out}$ and $P_{p,in}$ represent the static pressure at the outlet and inlet of the pump; $\rho_{p,in}$ represents the density at the inlet; m_f represents the mass flow rate through the pump; W_p represents the pump power; $\Delta h_{s,p}$ represents the isentropic enthalpy change across the pump; and η_p represents the pump isentropic efficiency.

An axial turbine has designed and delivered to our lab. Since it is still being commissioned, operational performance data of the turbine are taken from the manufacturer. The "TurbineMapGridRaw" template is chosen for the modelling of this component. A series of datasets including turbine speed, mass flow rate, volumetric efficiency, suction pressure and temperature, discharge pressure and temperature, efficiency and power are required. Figure 7 shows the turbine maps of corrected power and efficiency with corrected turbine speed at different pressure ratios. The pressure ratio, turbine speed and efficiency at the design conditions are 1.64, 40,000 rpm and 56.3%, respectively. GT-SUITE predicts the turbine speed and the pressure ratio at each timestep, and then searches the pre-processed turbine map to extract the mass flow rate and the isentropic efficiency for the simulation. The imposed outlet temperature is calculated using the enthalpy change across the turbine. The enthalpy change, and consequently the power produced by the turbine, are calculated as follows:

$$h_{t,out} = h_{t,in} - \Delta h_{s,t} \cdot \eta_t \tag{18}$$

$$W_t = \dot{m}_f \cdot \left(h_{t,in} - h_{t,out} \right) \tag{19}$$

$$\Delta h_{s,t} = c_p \cdot T_{total,in} \cdot \left(1 - \mathrm{P_r}^{\frac{1-\gamma}{\gamma}} \right) \tag{20}$$

$$T_{total,in} = T_{t,in} + \frac{u_{t,in}^2}{2 \cdot c_p} \tag{21}$$

where $h_{t,out}$ and $h_{t,in}$ represent the specific enthalpy at the outlet and inlet of the turbine; $\Delta h_{s,t}$ represents the isentropic enthalpy change across the turbine; Pr represents the pressure ratio across the turbine; $T_{total,in}$, $T_{t,in}$ and $u_{t,in}$ represent the total temperature, temperature and velocity at the turbine inlet; c_p and γ represent the specific heat capacity and specific heat ratio of the incoming gas; W_t represents the power produced by the turbine; and η_t represents the turbine isentropic efficiency.

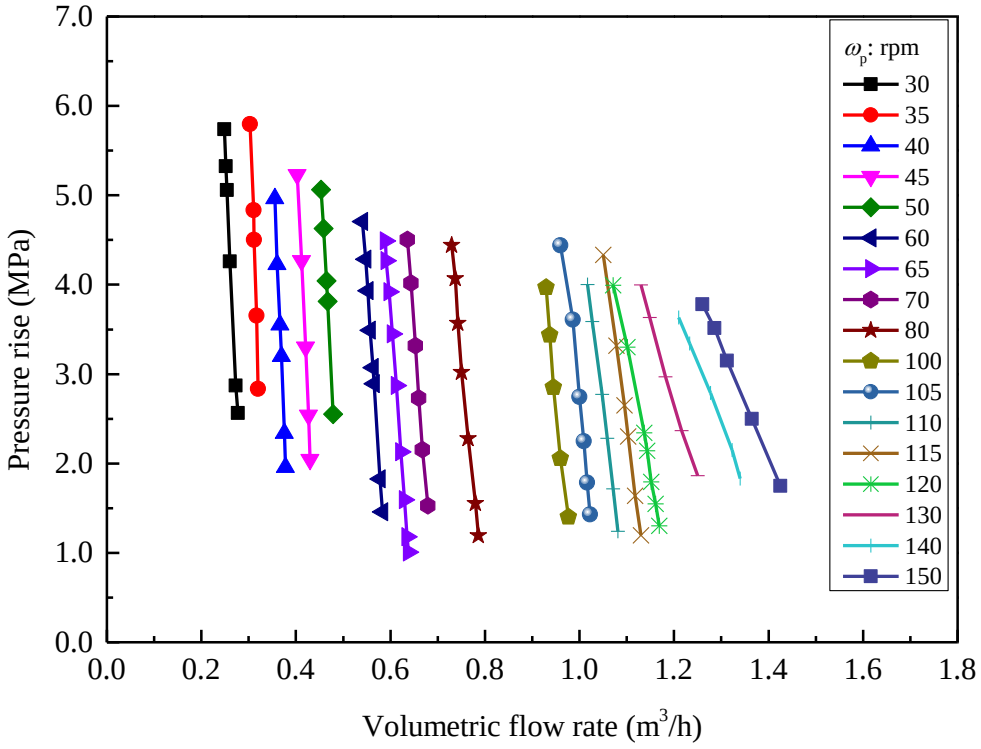


Fig. 6. Pump map: pressure rise with volumetric flow rate at different pump speeds.

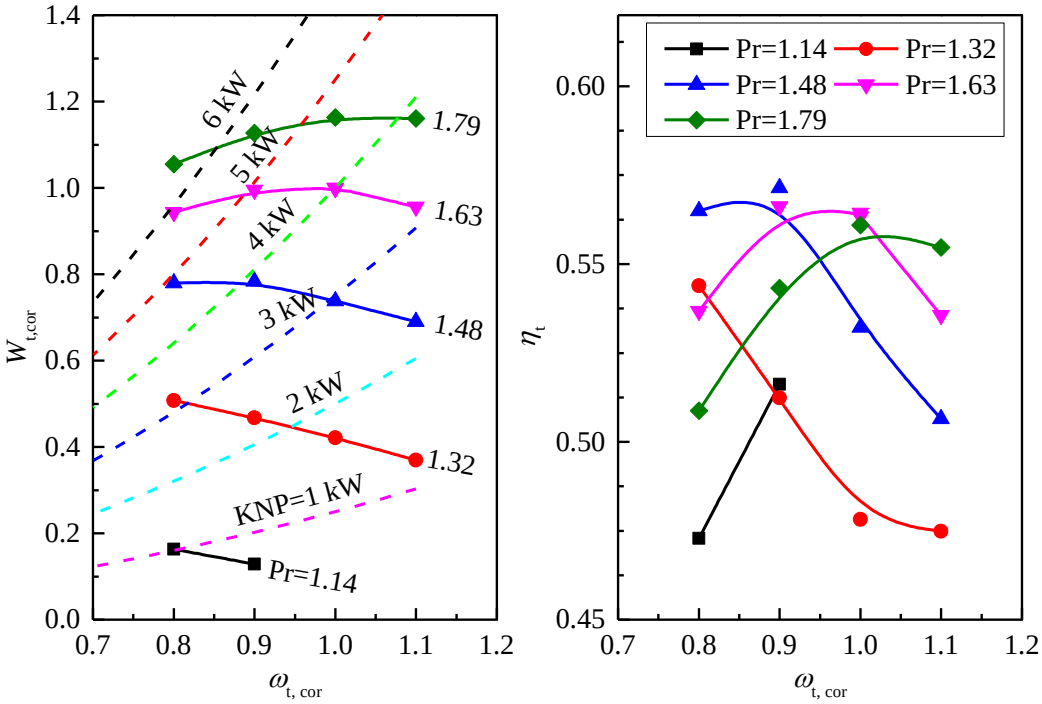


Fig. 7. Turbine maps: corrected power and efficiency as a function of corrected speed at different pressure ratios.

(4) Other component models:

The receiver is taken as a 10-L container. All pipes are modelled based on measured diameters and lengths. The inner diameter of high-pressure pipes is 12 mm and that of low-pressure pipes is 18 mm. Exhaust bypass and turbine bypass circuits are added in system models. Fluid properties are initialized by the initialization part using the boundary temperature and pressure. A performance module is also added for auto-calculation of system performance mainly including the net power output and the thermal efficiency.

The flow model used in the pipes and the flow-splits involves the solution of the Navier-Stokes equations [51], namely the conservation of continuity as shown in Eq. (22), the conservation of energy as shown in Eq. (23) for the explicit solver and Eq. (24) for the implicit solver, and the conservation of momentum equation as shown in Eq. (25). These equations are solved in one dimension, which means that all quantities are averages across the flow direction:

$$\frac{\mathrm{d}m}{\mathrm{d}t} = \sum \dot{m} \tag{22}$$

$$\frac{\mathrm{d}\left(m \cdot e\right)}{\mathrm{d}t} = -P \cdot \frac{\mathrm{d}V}{\mathrm{d}t} + \sum\left(\dot{m} \cdot H\right) - \alpha \cdot A_{\mathrm{s}} \cdot \left(T_{\mathrm{f}} - T_{\mathrm{w}}\right) \tag{23}$$

$$\frac{\mathrm{d}\left(\rho \cdot H \cdot V\right)}{\mathrm{d}t} = \sum\left(\dot{m} \cdot H\right) + V \cdot \frac{\mathrm{d}P}{\mathrm{d}t} - \alpha \cdot A_{\mathrm{s}} \cdot \left(T_{\mathrm{f}} - T_{\mathrm{w}}\right) \tag{24}$$

$$\frac{\mathrm{d}\dot{m}}{\mathrm{d}t} = \frac{\mathrm{d}P \cdot A + \sum\left(\dot{m} \cdot u\right) - 4 \cdot C_{\mathrm{f}} \cdot \frac{\rho \cdot u \cdot |u|}{2} \cdot \frac{\mathrm{d}x \cdot A}{D_{\mathrm{eq}}} - K_{\mathrm{p}} \cdot \left(\frac{\rho \cdot u \cdot |u|}{2}\right) \cdot A}{\mathrm{d}x} \tag{25}$$

where $\dot{m}$ denotes the mass flow rate of the fluid; m means the mass of the volume; e means the total specific internal energy; V means volume; H means the total specific enthalpy; α means the heat transfer coefficient; T_{f} and T_{w} represent the fluid temperature and the wall temperature, respectively; A_{s} means the heat transfer area; A means the cross-sectional flow area; u means the velocity at the boundary; C_{f} means the Fanning friction factor; K_{p} means the pressure loss coefficient; dx means the discretization length; dP means the pressure differential across dx.

2.2.2. Model calibration

The CTPC models are calibrated with experimental data, however, using an expansion valve. All current tests are being conducted using an expansion valve, which temporarily replaces the turbine until this is commissioned. Experimental results of different system configurations have been reported in Ref. [39] for steady-state thermodynamic performance evaluations; investigations of dynamic

characteristics have also been reported; see Refs. [40-42]. During the calibration exercise, an assumed constant efficiency is assigned to the turbine. The turbine speed varies to mimic the experiment of varying expansion valve opening, although this may lead to small differences in the expansion process, which affects the valve inlet and valve outlet temperatures, and further influences the cooling water outlet temperature. Figure 8 compares experimental data and simulation results for primary parameters such as pressure, temperature and mass flow rate. It is obvious that all these variables match well with the test data. Relative errors are calculated for steady state values. The maximum relative errors of valve inlet pressure, valve outlet pressure, mass flow rate, pump inlet temperature, pump outlet temperature, valve inlet temperature and cooling water outlet temperature are 4.1%, 1.2%, 0.7%, 1.1%, 1.5%, 9.2% and 7.2%, respectively. Therefore, the CTPC models are highly accurate and reliable for the following research as virtual test benches.

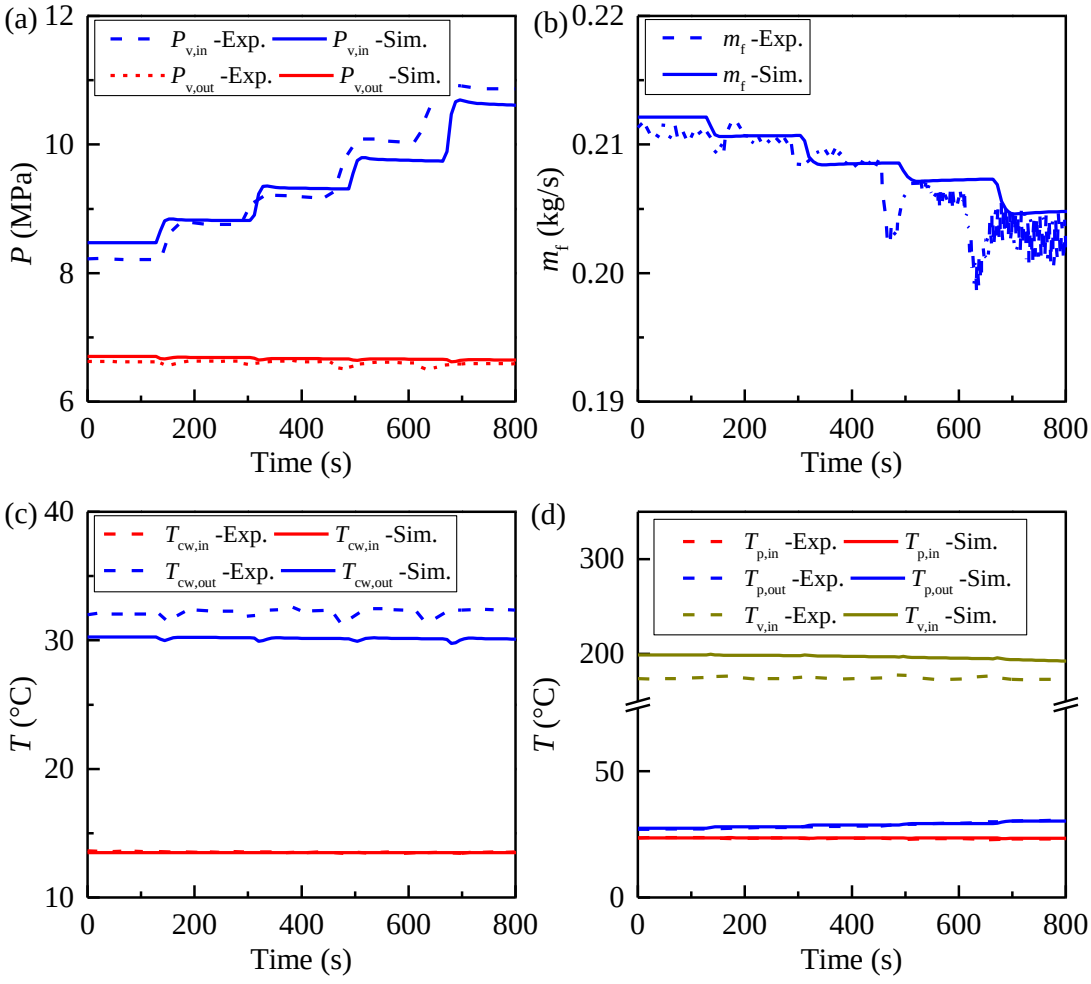


Fig. 8. CTPC model calibration: (a) pressure; (b) mass flow rate; (c) cooling water temperature; (d) temperature of CO_2.

3. Transient performance predictions

After individual component modelling and calibration, the ICE and CTPC models are coupled through a “FlowCircuitSplitter” template to simulate the transient system performance as per Figure 1, where this is denoted by “Engine-WHR-Connection”. The introduction of the “FlowCircuitSplitter” template in GT-SUITE is based on the following consideration: 1) the ICE model requires an explicit solver to predict pressure pulsations that occur in engine air flows and fuel injection systems. However, an implicit solver is applied to the CTPC models since high frequency pressure fluctuations are not of interest. 2) The exhaust gas acts as one of the heat sources for the CTPC systems, therefore it flows from the tailpipe to the slave side of the gas heater. If the ICE model is directly connected to the CTPC models through pipes, only one type of solver can be imposed to the exhaust circuit, which leads to a slow simulation speed. 3) The “FlowCircuitSplitter” template makes it possible to connect two individual flow circuits that use either different solvers or different time steps with the same solver. A PID controller is embedded to ensure the automatic data interaction such as mass flow rate, fluid concentrations, pressure and temperature. Moreover, coupling method could be selected as two-way coupling and one-way coupling. The former one could realize the feedback of backpressure calculated in the CTPC circuit to the ICE model while the latter avoids backpressure feedback. In current work, one-way coupling is chosen, and additional backpressure is ignored at the initial exploration stage.

3.1. CTPC control strategy

For combined simulation, the operating strategy of the CTPC systems needs to be identified first since it serves as a passive system in the coupled system. Figure 9 shows the control strategy of the CTPC system applied here. The corresponding controller models could be seen in Figure 4.

Based on the controllable variables, system control could be divided into four parts: 1) exhaust control through the bypass valve; 2) turbine control through the turbine bypass circuit and speed control; 3) pump control through its speed; and 4) cooling water control of the flow rate. Therefore, based on the states of these variables, three operating modes of the CTPC system are defined as stop mode, startup mode and power mode.

Stop mode (Mode 1): The CTPC system enters a stop mode when engine exhaust energy is inadequate to drive it. Therefore all the exhaust gas is bypassed and discharged to the ambient environment. In this case, pump and turbine keeps zero speed and no cooling water is needed.

However, if the average exhaust temperature ($\overline{T}_{exh}$) could maintain a higher value than the pre-set one ($\overline{T}_{exh,set}$) within at least a period (t_1), the CTPC could exit this mode and enter a startup mode.

Startup mode (Mode 2): The CTPC completes the startup of both the pump and the turbine. When the CTPC enters this mode, the pump gets started at an initial speed ($\omega_{p,0}$). At the same time, the cooling water circuit is turned on to realize an initial flow rate ($m_{cw,0}$). The turbine can only be switched on until the average turbine inlet pressure ($\overline{P}_{t,in}$) rises to a pre-set value ($\overline{P}_{t,in,set}$) and lasts for at least some time (t_2). The final turbine speed is around the set value of ω_t.

Power mode (Mode 3): In this mode, there is net power output of the CTPC system. Unlike ORC systems, there is no concern on the droplet formation at the inlet of the turbine since CO_2 experiences a single supercritical heating process in the gas heater. After several trials, we found that the CTPC could maintain an almost steady pressure even faced with highly transient heat sources. Therefore, in the power mode, in order to obtain a higher turbine inlet pressure and furthermore net power output, a control strategy is implemented through adjusting pump speed when turbine speed is steady and turbine inlet pressure shows a stable trend. Turbine inlet pressure variation ($\Delta\overline{P}_{t,in}$) is used to detect steady state and when $\Delta\overline{P}_{t,in}$ is less than the pre-set threshold $\Delta\overline{P}_{t,in,set}$ for at least a period of t_3, the pump speed controller (PID 1) is activated. Otherwise, the system remains at its current state. Cooling water control occurs when condenser inlet pressure ($P_{c,in}$) exceeds the pre-set value ($P_{c,in,set}$). Only the flow rate of the cooling water varies through PID 2 controller. This is reasonable because it is hard to lower the inlet temperature of the cooling water in a real scenario while adjusting the flow rate is much more feasible. When exhaust energy falls and becomes insufficient, the CTPC system switches to the stop mode.

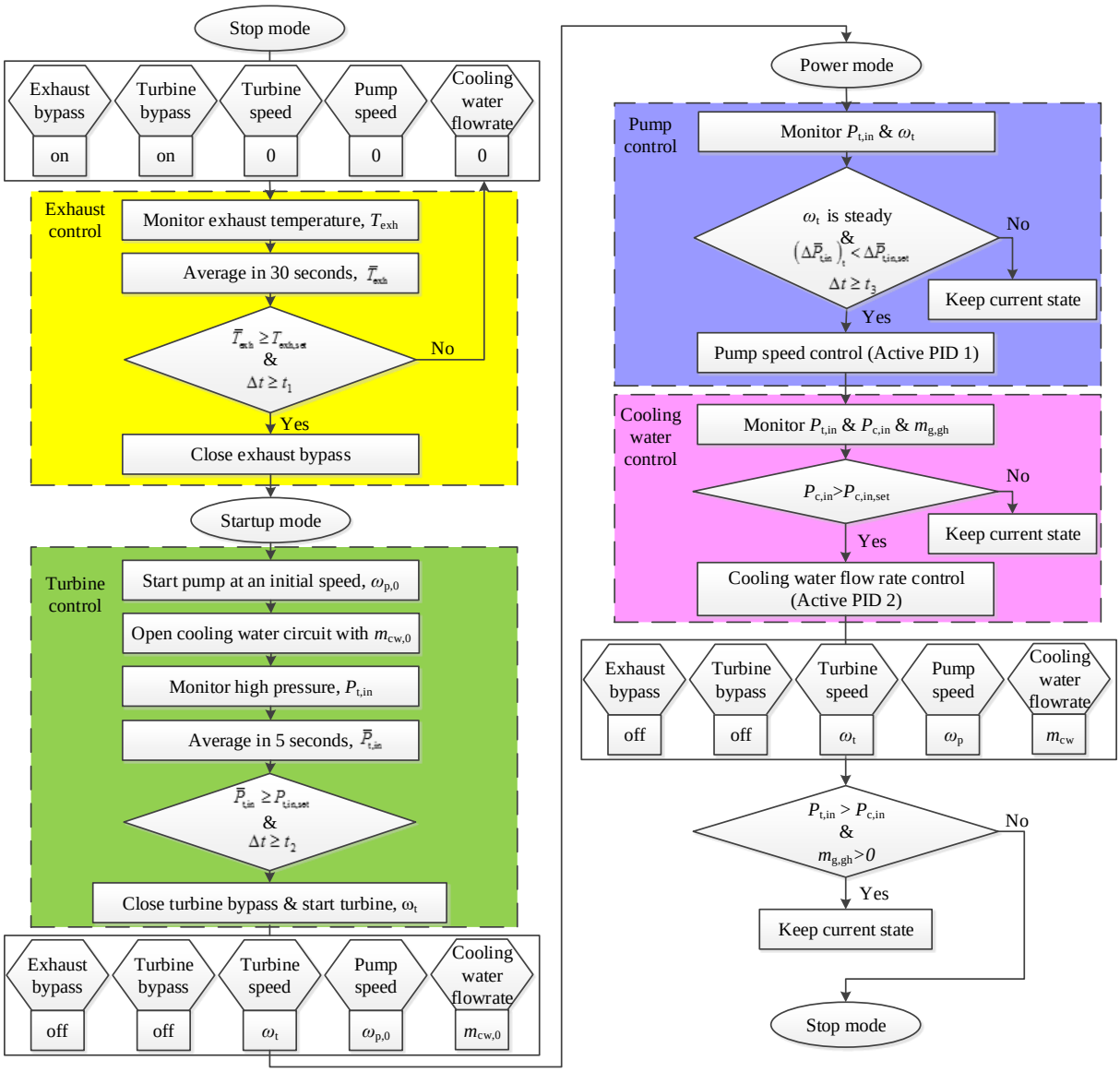


Fig. 9. Control strategy of CTPC systems.

Figure 10 illustrates the proposed control scheme for the CTPC systems. Based on the control strategy, two control loops are included: the outer loop for mode switch, and the inner loop for actuators and power control. PID controllers are applied for pump speed and cooling water control. Owing to the generic nature of a PID controller, the gains should be calibrated to reach the target value. The most common approach for finding good gain values is by trial-and-error, typically known as control calibration. However, it is time consuming to run many trial-and-error tests, but also requires hardware installed on a plant which was not possible in our case. Therefore, an analytical method has been adopted to find the proportional and integral gains (the derivative gain is typically ignored). Since the equations of a PI controller are complementary to a first-order linear response of a plant, step

changes are imposed in the experiment to identify the corresponding dynamic responses of the CTPC system and the output ratio (characterized as the ratio of the change in the output signal to the change in the input signal when the input signal is stepped) and the time constant are specified. These two parameters are provided to the PID controller template in GT-SUITE software, which analytically calculates the complementary proportional and integral gains. The final controller models are shown in Eq. (26) for the pump speed control and Eq. (27) for the cooling water control.

$$u(t) = 1.887 \cdot e(t) + 0.255 \cdot \int_0^t e(t)\mathrm{d}t \tag{26}$$

$$u(t) = -3.303 \cdot e(t) - 0.043 \cdot \int_0^t e(t)\mathrm{d}t \tag{27}$$

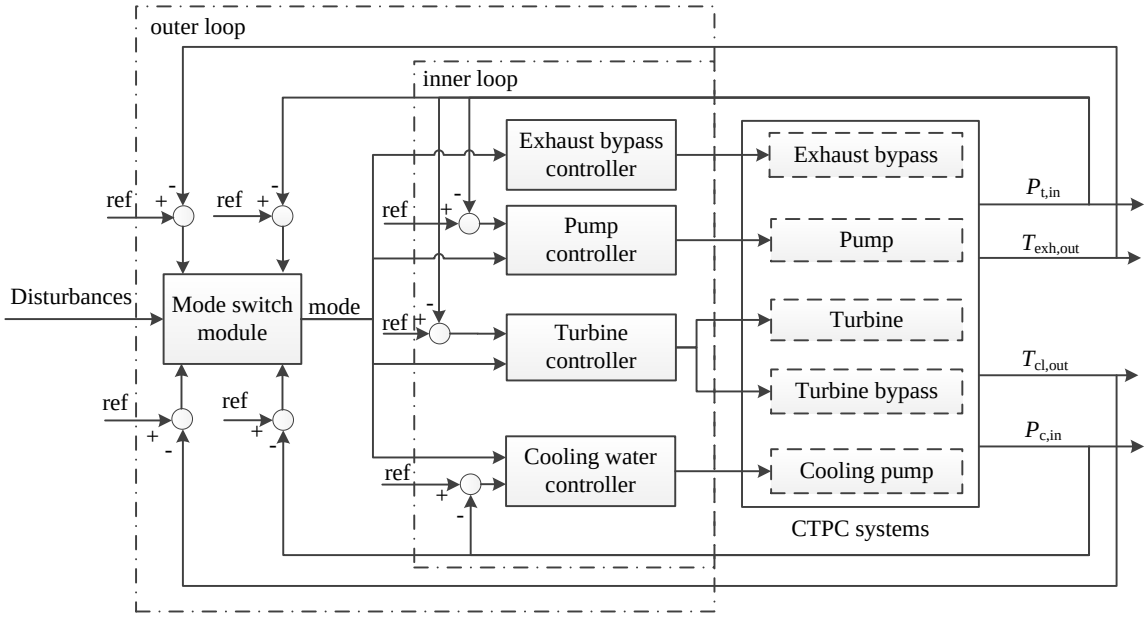


Fig. 10. Control structure of CTPC systems.

3.2. CTPC performance prediction

The present research aims to examine the dynamic behaviour of the CTPC systems under a driving cycle and to illuminate further directions for system optimization, with the expectation of laying the foundation for fully-transient studies of CTPC systems. A cruise driving cycle of heavy-heavy duty driving cycle (HHDDT) is selected for transient analysis. Figure 11 depicts the parameters under HHDDT_cruise cycle which lasts for 2083 s: (a) vehicle speed, engine speed, engine torque, engine power and engine brake thermal efficiency (BTE); (b) mass flow rate and temperature of exhaust gas; and (c) volume flow rate and temperature of engine coolant. At the first glance, it is clear that the

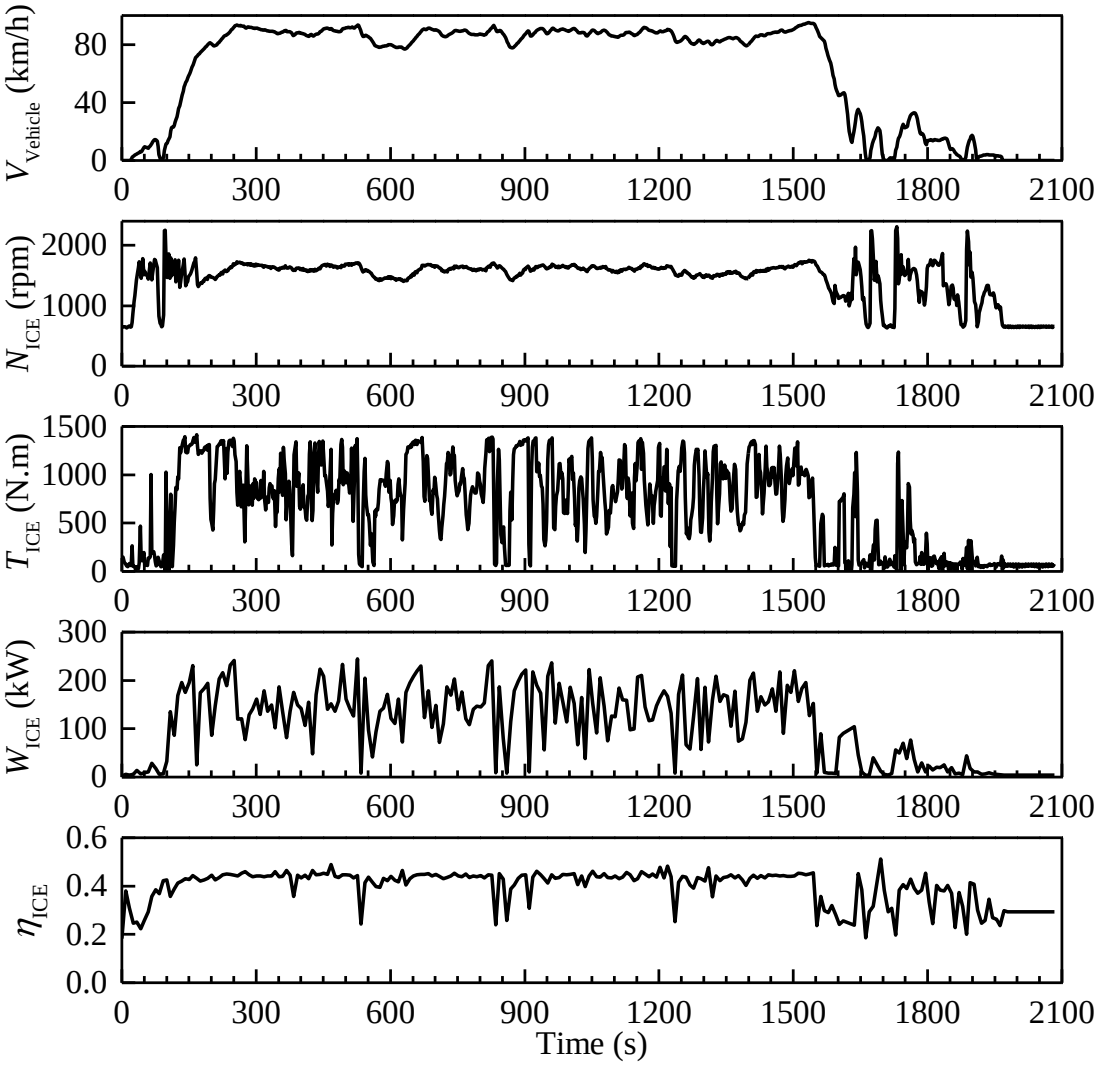
vehicle firstly speeds up, then cruises at around 86 km/h for more than 20 minutes and finally slows down to stop. All the other parameters show significant fluctuations during the whole cycle, even during the cruise period. To have a clear quantitative understanding, average values are calculated for the cruise period and results are given in Table 3. The engine achieves 42.8% brake thermal efficiency and outputs 142 kW brake power. The energy in the exhaust gases is calculated by Eq. (28) by assuming an acid dew point of 120 ºC, and amounts to 73.2 kW of thermal energy that is available can be recovered. As for the engine coolant, its energy is calculated as 45.9 kW through Eq. (29). These transient profiles are the boundary conditions of the CTPC systems since the exhaust and coolant act as the heat sources for the bottoming CTPC systems.

$$Q_{\mathrm{exh}} = \int \dot{m}_{\mathrm{exh}} \cdot h\left(T_{\mathrm{exh}}, P_{\mathrm{exh}}\right) \mathrm{d}t - \int \dot{m}_{\mathrm{exh}} \cdot h\left(T_{\mathrm{acid}}, P_{\mathrm{exh,out}}\right) \mathrm{d}t \tag{28}$$

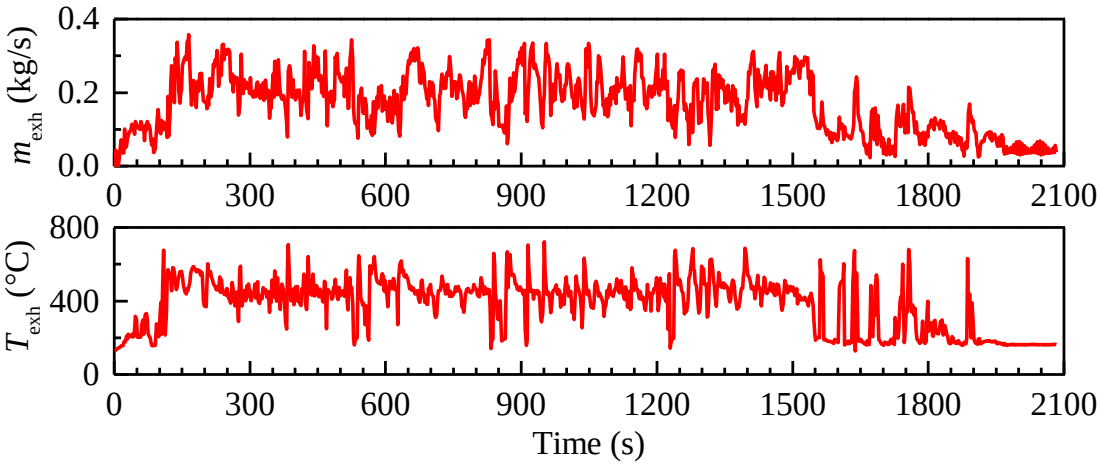
$$Q_{\mathrm{cl}} = \int \dot{m}_{\mathrm{cl}} \cdot c_{\mathrm{p,cl}} \cdot \left(T_{\mathrm{cl,in}} - T_{\mathrm{cl,out,exp}}\right) \mathrm{d}t \tag{29}$$

Table 3. Average values of the main parameters of the engine during cruise period.

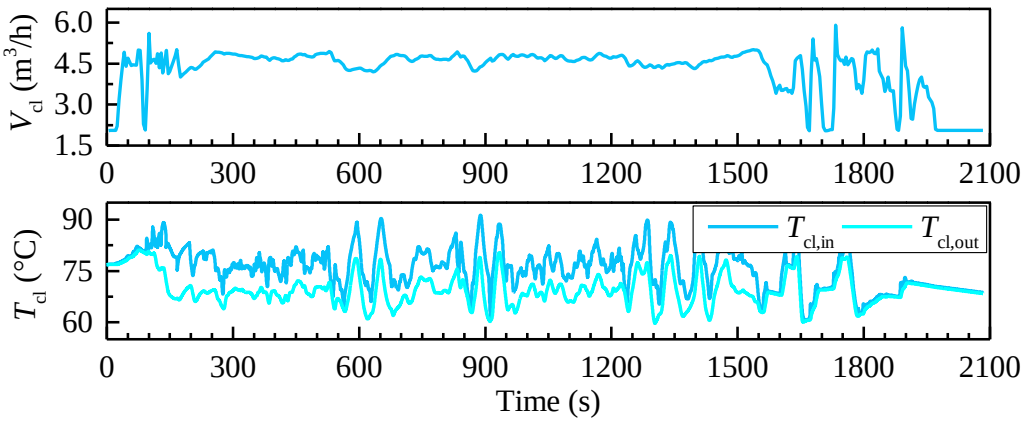
Parameters	**Unit**	**Value**
Engine power	kW	142
Engine brake thermal efficiency	%	42.8
Exhaust temperature	ºC	443
Exhaust mass flow rate	kg/s	0.21
Exhaust available energy	kW	73.2
Coolant inlet temperature	ºC	69
Coolant outlet temperature	ºC	77
Coolant flow rate	m^3/h	4.6
Coolant available energy	kW	45.9



(a) Vehicle speed, engine speed, torque, brake power and brake thermal efficiency.



(b) Mass flow rate and temperature of exhaust-gas stream.



(c) Volume flow rate and temperature of engine coolant.

Fig. 11. Parameters of vehicle, engine, exhaust and coolant under HHDDT_cruise cycle.

Taking the PR-CTPC system as an example, Figure 12 demonstrates the predicted transient responses under the HHDDT_cruise cycle. Main variables including the controller outputs, temperatures, pressures, mass flow rate and efficiencies are presented. The initial cooling water temperature and flow rate are set as 20 ºC and 5 m^3/h, respectively. It is noted that the condensation process in such CTPC systems depends strongly on the environmental (or ambient) temperature through which a truck is moving. If the ambient temperature is lower than 20-25 °C, the ambient air can be used as the heat sink. There are many global regions where the ambient temperature satisfies this condition, and in regions where the temperatures are close to this value, forced convection from the surrounding air and fans, along with corresponding controllers (PID, MPC, etc.) can be installed to control the flow rate of the cooling air and therefore ensure condensation within the system. Such a design would be similar to radiators on conventional vehicles, but smaller in size given the lower cooling duties. Therefore, it is considered reasonable to set the initial cooling water temperature to 20 ºC. As is observed, the PR-CTPC system keeps stopped when the vehicle starts up. With the climbing of exhaust energy, the PR-CTPC system enters the startup mode at 66 s and power mode from 144 s successively. Almost after 1600 s, the PR-CTPC system returns to the stop mode since the vehicle speeds down and consequently generates less waste energy. Correspondingly, based on the working principle of these controllers, at the end of the startup mode, the pump speed changes from 0 rpm to 80 rpm and the turbine operates at 32000 rpm.

Turning to the details of the fifth subgraph, it is apparently seen that turbine inlet pressure ($P_{t,in}$) goes down significantly at 78 s when turbine bypass valve is closed. This could be explained that

before 78 s, $P_{t,in}$ indicates the pressure through the bypass circuit while at the same time the turbine circuit is cut off and maintains a rather smaller pressure. Therefore, $P_{t,in}$ firstly decreases when it switches to the turbine circuit. Afterwards, $P_{t,in}$ climbs up to almost 8 MPa with the increase of exhaust mass flow rate and temperature as shown in Figure 11(b). It should be noted that from about 165 s, $P_{t,in}$ shows an approximate steadiness although exhaust conditions fluctuate dramatically, showing a strong robustness of CTPC against transient heat sources. Without any other adjustment, the PR-CTPC system would operate at this pressure and output little net power.

Aiming at obtaining the maximum net power output, control strategy is implemented. From roughly 250 s, pump speed controller is activated and hence pump speed shows a jump from 80 rpm to 150 rpm. $P_{t,in}$ leaps to more than 12.5 MPa and oscillates slightly until the PR-CTPC system changes to the stop mode. Although the target $P_{t,in}$ is set as 15 MPa, the pump speed cannot be adjusted to a higher value because a threshold is preset and the maximum speed is limited to 150 rpm. Moreover, turbine outlet pressure (which keeps around 7 MPa) and temperatures stabilize at their own values during the power mode, indicating the strong ability of the PR-CTPC system to operate continuously and safely even faced with transient heat sources.

According to the last two subgraphs in Figure 12, we can see that pump power consumption (W_p), turbine power production (W_t), net power output (W_{net}) and thermal efficiency (η_{th}) show similar trends with $P_{t,in}$. The average thermal efficiency of the PR-CTPC system during the power mode is calculated as 6.5%. Averaged values for W_p, W_t and W_{net} are 2.6 kW, 7.2 kW and 4.6 kW, respectively. It is worth noticing that both the isentropic efficiencies of the pump and the turbine are just around 50% during the power mode, which causes the deterioration of net power output. To show the contribution to the original engine, several indicators are defined as follows.

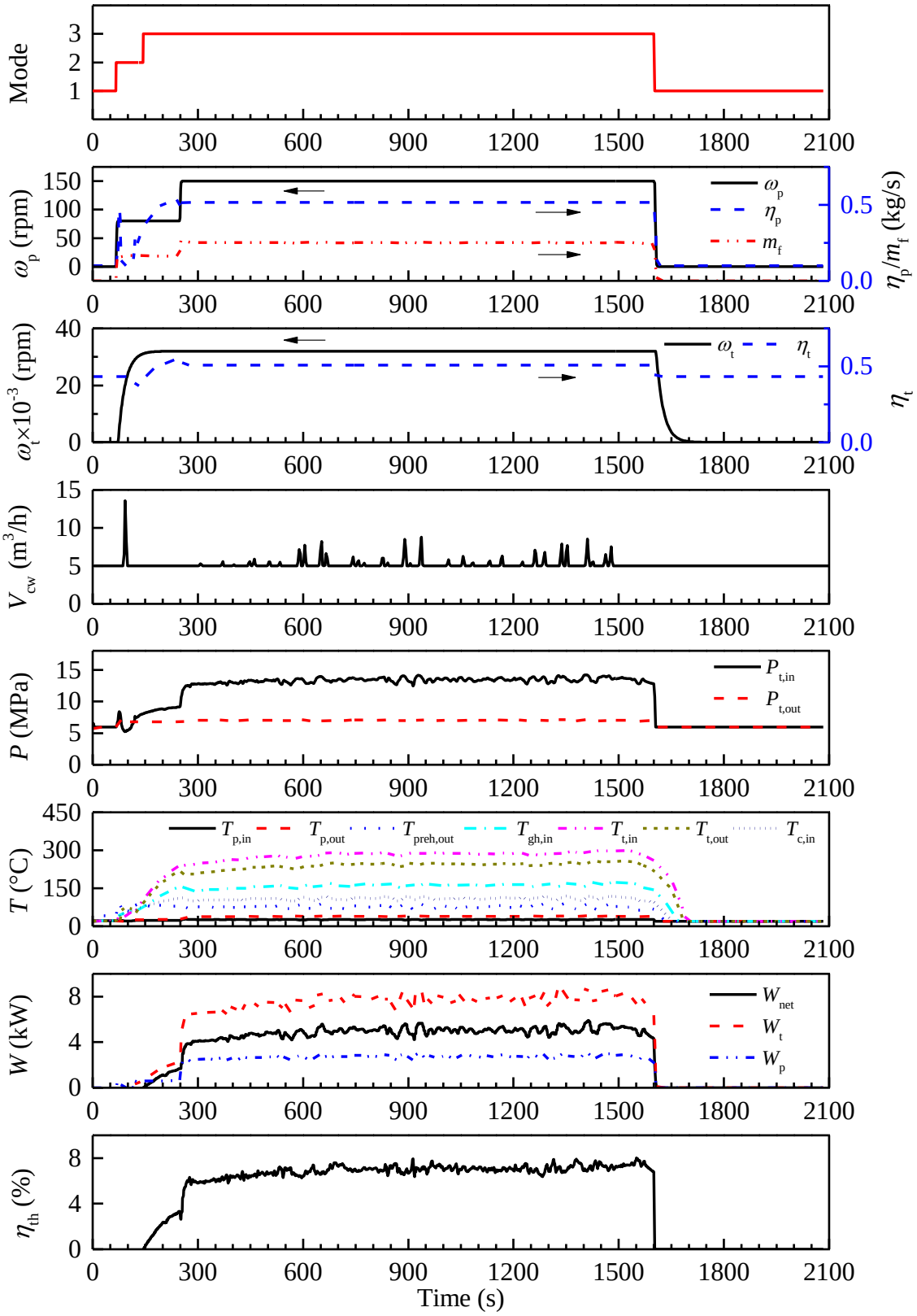


Fig. 12. Transient responses of PR-CTPC system under HHDDT_cruise cycle.

The absolute improvement in the engine brake thermal efficiency during power mode is given by:

$$\Delta\eta_{\mathrm{ICE}} = \eta_{\mathrm{ICE}}^{'} - \eta_{\mathrm{ICE}} = \frac{W_{\mathrm{net}} + W_{\mathrm{ICE}}}{Q_{\mathrm{fuel}}} - \frac{W_{\mathrm{ICE}}}{Q_{\mathrm{fuel}}} = \frac{W_{\mathrm{net}}}{Q_{\mathrm{fuel}}} = \frac{W_{\mathrm{net}}}{W_{\mathrm{ICE}}} \cdot \eta_{\mathrm{ICE}} \tag{30}$$

and the corresponding relative improvement in the engine brake thermal efficiency is:

$$\Delta\eta_{\mathrm{r}} = \frac{\Delta\eta_{\mathrm{ICE}}}{\eta_{\mathrm{ICE}}} = \frac{\eta_{\mathrm{ICE}}^{'} - \eta_{\mathrm{ICE}}}{\eta_{\mathrm{ICE}}} = \frac{W_{\mathrm{net}}}{W_{\mathrm{ICE}}} \tag{31}$$

The absolute improvement in the engine brake thermal efficiency over the whole driving cycle is:

$$\Delta\eta_{\mathrm{ICE,dc}} = \Delta\eta_{\mathrm{ICE}} \cdot \xi_{\mathrm{power}} = \Delta\eta_{\mathrm{ICE}} \cdot \frac{t_{\mathrm{power}}}{t_{\mathrm{dc}}} \tag{32}$$

and the corresponding relative improvement over the whole driving cycle is given by:

$$\Delta\eta_{\mathrm{r,dc}} = \Delta\eta_{\mathrm{r}} \cdot \xi_{\mathrm{power}} = \Delta\eta_{\mathrm{r}} \cdot \frac{t_{\mathrm{power}}}{t_{\mathrm{dc}}} \tag{33}$$

where ξ_{power} denotes the percentage of power mode, defined as the ratio of lasting time of power mode (t_{power}) and the whole driving cycle (t_{dc}).

Furthermore, the utilization rate of thermal energy from the exhaust-gas stream is defined as:

$$U_{\mathrm{exh}} = \frac{\int \dot{m}_{\mathrm{exh}} \cdot h\left(T_{\mathrm{exh}}, P_{\mathrm{exh}}\right)\mathrm{d}t - \int \dot{m}_{\mathrm{exh}} \cdot h\left(T_{\mathrm{exh,out}}, P_{\mathrm{exh,out}}\right)\mathrm{d}t}{\int \dot{m}_{\mathrm{exh}} \cdot h\left(T_{\mathrm{exh}}, P_{\mathrm{exh}}\right)\mathrm{d}t - \int \dot{m}_{\mathrm{exh}} \cdot h\left(T_{\mathrm{acid}}, P_{\mathrm{exh,out}}\right)\mathrm{d}t} \tag{34}$$

and the utilization rate of thermal energy from the engine coolant stream is:

$$U_{\mathrm{cl}} = \frac{\int \dot{m}_{\mathrm{cl}} \cdot c_{\mathrm{p,cl}} \cdot \left(T_{\mathrm{cl,in}} - T_{\mathrm{cl,out,sim}}\right)\mathrm{d}t}{\int \dot{m}_{\mathrm{cl}} \cdot c_{\mathrm{p,cl}} \cdot \left(T_{\mathrm{cl,in}} - T_{\mathrm{cl,out,exp}}\right)\mathrm{d}t} \tag{35}$$

Figure 13 presents detailed information about the percentage of each mode in the PR-CTPC system during the HHDDT_cruise cycle. It matches with the first subgraph of Figure 12. The power mode accounts for 69.9%, which seems considerable. After calculation, the PR-CTPC system could achieve 1.4% of $\Delta\eta_{\mathrm{ICE}}$, 3.3% of $\Delta\eta_{\mathrm{r}}$, 1.0% of $\Delta\eta_{\mathrm{ICE,dc}}$ and 2.3% of $\Delta\eta_{\mathrm{r,dc}}$. Mode switch of the PR-CTPC system causes discount of its contribution. Large proportion of power mode during a transient driving cycle would facilitate the application of the PR-CTPC system. This calls for the trucks to cruise as much as possible therefore the PR-CTPC system is much more attractive to long-haul trucks.

In order to have a full understanding of the potential of the PR-CTPC system, outlet temperatures of heat sources in PR-CTPC system under HHDDT_cruise cycle are demonstrated in Figure 14. These curves reflect the utilization rates of heat sources. Although the simulated outlet temperature of engine

coolant shows a similar trend with the measured one (engine requirement), there is some delay with the temperature and the calculated average utilization rate of engine coolant is 72.8%. At the same time, turning to the details of the exhaust curve, the average outlet temperature (around 260 ºC), is rather higher than the acid dew temperature (120 ºC). It indicates the PR-CTPC system could only partially recover the exhaust energy. Only 48.9% of the exhaust energy is utilized in the current system. Insufficient recovery of waste energy also leads to performance reduction of the PR-CTPC system. Modified heat exchangers and turbomachinery with better performance are required.

Based on the above, current PR-CTPC system could be further optimized to realize better contribution to engine thermal efficiency through three approaches: 1) applying this system to long-haul trucks to extend the percentage of power mode; 2) optimizing the components to fully recover the waste energy; and 3) simply improving the isentropic efficiencies of turbine and pump to increase net power output even at the same utilization rates of heat sources.

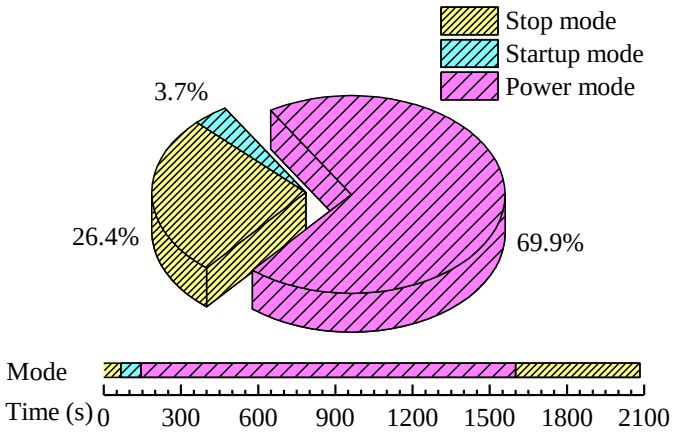


Fig. 13. Percentage of each mode in PR-CTPC system under HHDDT_cruise cycle.

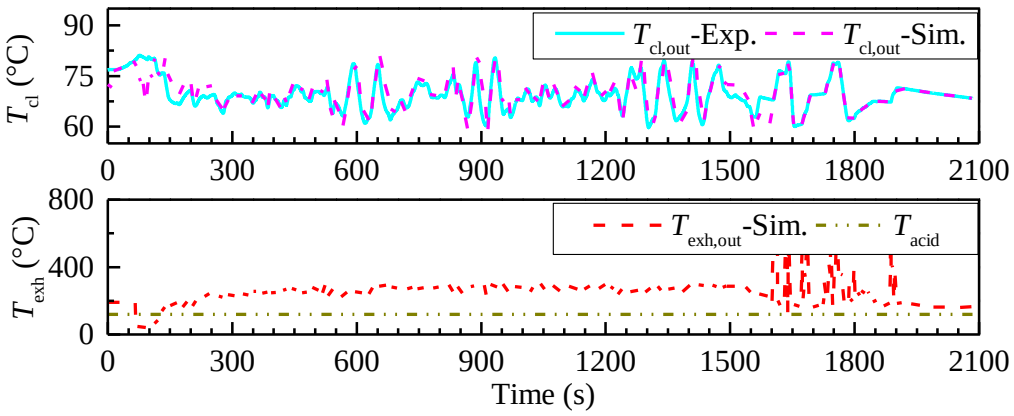


Fig. 14. Outlet temperature of heat sources in PR-CTPC system under HHDDT_cruise cycle.

Three other types of the CTPC system, i.e. CTPC, R-CTPC and P-CTPC, have also been examined. For the sake of avoiding redundancy, predicted transient responses are not displayed here and only performance comparison of the four systems is listed in Table 4. From the given data, the PR-CTPC possesses the largest net power output of 4.6 kW, which is increased by 138.0%, 54.9% and 40.2% when compared with CTPC, R-CTPC and P-CTPC, respectively. Also, the PR-CTPC makes the best contribution to the original engine which can realize 2.3% relative improvement over the whole driving cycle. The CTPC obtains a considerable utilization rate of exhaust gas, which is almost forty percentages more than the PR-CTPC. If merely a recuperator is added, the ability of exhaust energy recovery is reduced with a small portion, showing from 88.0% to 72.9%. However, if adding a preheater at the same time, the utilization rate of exhaust falls largely. Consequently, the PR-CTPC system should employ heat exchangers with more heat transfer areas and turbomachinery of larger scale to fully extract energy from both exhaust and engine coolant. Among these four layouts, the PR-CTPC still outperforms from the perspective of power performance.

Table 4. Performance comparison of four CTPC systems under HHDDT_cruise cycle.

Parameters	**Unit**	**CTPC**	**R-CTPC**	**P-CTPC**	**PR-CTPC**
Q_{pre}	kW	0	0	34.0	33.4
Q_{gh}	kW	64.4	53.4	48.9	35.8
Q_{rec}	kW	0	25.0	0	35.5
Q_c	kW	62.4	50.1	79.6	64.3
W_p	kW	1.4	1.6	1.7	2.6
W_t	kW	3.3	4.6	5.0	7.2
W_{net}	kW	1.9	3.0	3.3	4.6
η_{th}	%	2.9	5.4	3.9	6.5
$\Delta\eta_r$	%	1.4	2.1	2.7	3.3
$\Delta\eta_{ICE}$	%	0.6	0.9	1.2	1.4
$\Delta\eta_{r,dc}$	%	0.9	0.2	1.9	2.3
$\Delta\eta_{ICE,dc}$	%	0.4	0.6	0.8	1.0

U_{exh}	%	88.0	72.9	66.8	48.9
U_{cl}	%	0	0	74.2	72.8

4. Analysis of potential improvements

As mentioned above, the PR-CTPC system can be optimized further. From the viewpoint of the system itself, component optimization and cooling capacity enhancement are the two main approaches. The following investigation is conducted without the consideration of heat exchanger optimization due to the complicated structure modification and lack of experimental tests of physical components.

4.1. Pump and turbine efficiency

Pump and turbine are important in the systems since they directly relate to the net power output. As depicted in Figure 12, current pump and turbine could operate with nearly 50% isentropic efficiencies under the HHDDT_cruise cycle. There is no doubt that the system would obtain better performance if the pump and turbine could realize a higher isentropic efficiency. The potential of performance improvement is examined through improving pump and turbine efficiency individually or simultaneously. In order to maintain the same boundary conditions, enough cooling capacity is implemented with the cooling water inlet temperature of 20 ºC and flow rate of 10 m^3/h. Table 5 lists the calculated results after simulations of the PR-CTPC systems under the HHDDT_cruise cycle.

At the onset, the system with original pump and original turbine (OPOT) shows a slightly increment in net power output than that displayed in Table 4 thanks to an extra flow rate of cooling water which brings an enhanced cooling capacity. By adopting a modified pump (MP), the PR-CTPC system consumes less pump power and reduces back work ratio. As shown in Table 5, pump power consumption decreases from 2.7 kW to 1.9 kW if the average pump isentropic efficiency is improved from 51.5% to 71.9%. By designing a turbine with a higher isentropic efficiency, i.e. employing a modified turbine (MT), the PR-CTPC system could produce 36.0% more power than the original one if the turbine could operate with an average efficiency of 71.0%. Therefore, optimizing pump and turbine efficiencies at the same time could bring substantial improvement of the PR-CTPC system. As shown in the MPMT data, the net power output improves by a little over 70.0% from 4.9 kW to 8.3 kW. And the contribution of the PR-CTPC system to the original engine largely rises to 4.2% for relative improvement during the whole

driving cycle and 1.8% for absolute improvement. Other operating conditions such as pressure and mass flow rate are almost the same for the four cases considered.

Table 5. Potential of performance improvement by pump and turbine modification.

Parameters	Unit	OPOT	MP	MT	MPMT
V_{cw}	m^3/h	10	10	10	10
$T_{cw,in}$	ºC	20	20	20	20
η_p	%	51.5	71.9	51.4	71.6
η_t	%	50.8	50.7	71.0	70.1
$P_{t,in}$	MPa	13.0	12.9	12.8	12.9
$P_{t,out}$	MPa	6.7	6.7	6.7	6.7
$T_{t,in}$	ºC	272	271	265	264
m_f	kg/s	0.25	0.25	0.25	0.24
W_p	kW	2.7	1.9	2.6	1.9
W_t	kW	7.6	7.5	10.3	10.2
W_{net}	kW	4.9	5.6	7.7	8.3
$\Delta\eta_r$	%	3.5	4.0	5.4	5.9
$\Delta\eta_{ICE}$	%	1.5	1.7	2.3	2.5
$\Delta\eta_{r,dc}$	%	2.4	2.8	3.8	4.2
$\Delta\eta_{ICE,dc}$	%	1.0	1.2	1.6	1.8

4.2. Cooling capacity

Cooling capacity needs to be considered since it decides the condensing pressure of the CTPC systems. Here, two sets of cases with cooling water at different inlet temperatures and flow rates are simulated and compared under the HHDDT_cruise cycle. Table 6 and Table 7 give the calculated results of performance improvement potential through solely changing cooling water inlet temperature and flow rate, respectively. Since the critical temperature of CO_2 is only 31.1 ºC, the inlet temperature of the

cooling water is set to be 25 ºC, 20 ºC, 15 ºC, 10 ºC and 5 ºC. The simulation is failed when adopting cooling water with the temperature of 25 ºC, indicating its infeasibility to accomplish a transcritical power cycle when cooling water temperature is above 25 ºC. Therefore, only four cases are shown in Table 6. It is apparently seen that the inlet temperature of the cooling water has great impacts on the condensing pressure. The condensing pressure decreases from 6.7 MPa to 5.2 MPa with the decline of cooling water temperature from 20 ºC to 5 ºC. This further brings a higher inlet density of CO_2 in the pump and hence the mass flow rate of CO_2 is increased while the turbine inlet temperature of CO_2 is lowered. Both the pump power consumption and turbine power production move upwards, however, the latter changes much more noticeably. That is why the net power output shows an increase.

Table 7 shows the results of increasing flow rate of cooling water from 4 m^3/h to 16 m^3/h with an interval of 2 m^3/h. It is obvious that the flow rate only brings little influences on the contribution of the PR-CTPC system since the relative improvement of engine brake thermal efficiency during the whole cycle is just around 2.4% for all the seven cases. Only small differences can be seen in the condensing pressure. It could maintain about 6.7 MPa condensing pressure if the flow rate is above 8 m^3/h while it upsurges to its critical pressure (7.4 MPa) if the cooling water is supplied at a flow rate of less than 4 m^3/h, meaning an insufficient cooling capacity. It demonstrates that the minimum flow rate could be implemented through the requirement of condensing pressure and no extra flow rate is needed. This will minimize the power consumption of cooling water supply. A good controller for cooling water is demanded in real applications.

Based on the analysis of Section 4.1 and Section 4.2, one could infer that the key point of system performance optimization is to improve pump and turbine efficiency. It could be explained from the following three aspects: 1) improvement of pump and turbine efficiency show a huge potential of contribution promotion; 2) cooling water flow rate has little impacts on performance improvement; 3) although inlet temperature of cooling water could uplift net power output, it seems not cost-effective to lower the temperature as much as possible in truck applications.

Table 6. Potential of performance improvement by lowering cooling water temperature.

Parameters	**Unit**	**Case 1**	**Case 2**	**Case 3**	**Case 4**
V_{cw}	m^3/h	10	10	10	10
$T_{cw,in}$	ºC	20	15	10	5

η_p	%	51.5	51.6	52.0	53.2
η_t	%	50.8	50.9	51.1	50.8
$P_{t,in}$	MPa	13.0	13.0	13.3	13.6
$P_{t,out}$	MPa	6.7	6.1	5.6	5.2
$T_{t,in}$	ºC	272	260	245	244
m_f	kg/s	0.25	0.25	0.26	0.27
W_p	kW	2.7	3.0	3.5	4.0
W_t	kW	7.6	8.5	9.7	11.0
W_{net}	kW	4.9	5.5	6.2	7.0
$\Delta\eta_r$	%	3.5	3.9	4.4	4.9
$\Delta\eta_{ICE}$	%	1.5	1.7	1.9	2.1
$\Delta\eta_{r,dc}$	%	2.4	2.7	3.1	3.5
$\Delta\eta_{ICE,dc}$	%	1.1	1.2	1.3	1.5

Table 7. Potential of performance improvement by increasing cooling water flow rate.

Parameters	**Unit**	**Case 1**	**Case 2**	**Case 3**	**Case 4**	**Case 5**	**Case 6**	**Case 7**
V_{cw}	m^3/h	4	6	8	10	12	14	16
$T_{cw,in}$	ºC	20	20	20	20	20	20	20
η_p	%	51.4	51.4	51.4	51.5	51.5	51.5	51.5
η_t	%	50.8	50.8	50.8	50.8	50.8	50.8	50.8
$P_{t,in}$	MPa	13.0	13.0	13.0	13.0	13.0	13.0	13.0
$P_{t,out}$	MPa	7.2	6.9	6.8	6.7	6.7	6.6	6.6
$T_{t,in}$	ºC	275	273	272	272	271	271	271
m_f	kg/s	0.25	0.25	0.25	0.25	0.25	0.25	0.25
W_p	kW	2.5	2.6	2.6	2.7	2.7	2.7	2.7
W_t	kW	7.0	7.3	7.4	7.6	7.6	7.7	7.7

W_{net}	kW	4.5	4.7	4.8	4.9	4.9	5.0	5.0
$\Delta\eta_r$	%	3.2	3.3	3.4	3.5	3.5	3.5	3.6
$\Delta\eta_{ICE}$	%	1.4	1.4	1.5	1.5	1.5	1.5	1.5
$\Delta\eta_{r,dc}$	%	2.2	2.3	2.4	2.4	2.5	2.5	2.5
$\Delta\eta_{ICE,dc}$	%	0.9	1.0	1.0	1.0	1.1	1.1	1.1

5. Conclusions

Most studies to-date on waste-heat recovery from heavy-duty truck engines have focused on Rankine cycle or organic Rankine cycle systems, either through simulation on different configuration layouts, working fluids and operating parameters, or tests for limited conditions to obtain typical steady-state performance. Similarly, recent research on carbon dioxide transcritical power cycle (CTPC) systems also focuses separately either on theoretical or experimental approaches. The transient characteristics of heat sources are not fully considered, which is critical in vehicle applications. The present study goes beyond earlier work by performing a joint modelling and experimental effort aiming to explore further the potential of CTPC waste-heat recovery systems for heavy-duty truck engines in operational scenarios closer to real applications of this technology. Detailed models of the internal combustion engine and CTPC are firstly developed and calibrated against experimental data in the 1-D simulation environment GT-SUITE. Control strategies for the CTPC systems are proposed to allow stable, safe and optimal operation. Performance is predicted for four alternative CTPC system layouts (basic CTPC system, recuperative CTPC system, preheated CTPC system, and CTPC system with both a preheater and a recuperator) under a selected (cruise) driving cycle.

The main conclusions from this work can be summarized as follows:

(1) CTPC waste heat recovery systems show strong robustness against highly transient heat sources and can maintain an almost steady pressure and temperature even during a driving cycle, i.e. have the ability to deliver a steady output power. Considering their potential for component miniaturization, CTPC systems are a promising alternative to ORC systems for mobile vehicle applications.

(2) Three operating modes are defined in relation to various driving cycles: stop mode, startup mode and power mode. Increasing the power mode percentage improves the final economy contribution of the CTPC systems, making long-haul trucks attractive for CTPC technology integration.

(3) Factor analysis suggests that the pump and turbine are the key components that should be optimized first, while the cooling water flow rate needs to be carefully controlled in order to reduce parasitic power consumption by the pump.

(4) The CTPC system with both a preheater and a recuperator outperforms the other three layouts and shows the most promising performance. With pump and turbine isentropic efficiencies as low as 50%, the system can improve fuel economy by 2.3% over the original engine in a whole heavy-heavy duty driving cycle. If the pump and turbine efficiencies were improved to about 70%, the contribution could be up to 4.2%.

Future work will concentrate on: 1) heat exchanger optimization to fully extract waste energy; and 2) two-way coupling of the engine and CTPC systems to have a better understanding of the impact caused by backpressure and weight addition, and also the impacts on vehicle aftertreatment systems.

Acknowledgement

This work was supported by National Key R&D Program of China (2017YFE0102800). The authors would also like to thank China Scholarship Council for a joint-PhD scholarship that supported Xiaoya Li for this research. The authors would also like to acknowledge the engineers from GT support for the help in software application. This work was also supported by the UK Engineering and Physical Sciences Research Council (EPSRC) [grant number EP/P004709/1].

Appendix A

Table A.1 summarizes the most recent RC/ORC technology developments from leading companies in applications related to long-haul trucks. One of the pioneers of this technology, Thermo Electron, simulated an ORC system recovering energy from the exhaust gases with Fluorinol-50 as the working fluid [12] and conducted two 1000-hour tests on a Mack 676 DE mainly focusing on system endurance [13]. Results revealed lifetime issues with each component and demonstrated an average relative fuel economy improvement of 12.5%. In 2012, Bosch [14] and Behr Thermal Systems [15] reported fuel consumption improvements of 4-5% and 2-6%, respectively, through recovering exhaust and EGR heat in long-haul vehicles using ethanol or water-based cycles. Two years later, Hino Motors [16] obtained a 7.5% improvement in fuel economy by collecting EGR, engine coolant (at an increased temperature of 105 ºC) and exhaust heat using hydro-fluoro-ether as the working fluid. Within the frame of the US Super Truck Program, intensive investigations were conducted by Cummins [17,18], Daimler [19], Volvo [18,20] and Eaton [21]. Focusing on DEs in the approximate size range of 350 kW, different heat sources, working fluids, system layouts, component types and integration methods were considered. Among which, road tests by Cummins [17,18] demonstrated the best absolute improvement of the engine thermal efficiency of 3.6% with an R245fa-based ORC system recovering exhaust and EGR energy. Volvo [18,20] also mounted the RC system on a truck and testing results showed 2% contribution to the fuel economy, while Daimler [19] focused on ethanol-based ORC system and Eaton [21] chose the engine coolant as the working fluid.

Table A.1. ORC implementations for long-haul trucks by some leading companies.

Year	Institution	Engine	ICE power (kW)	WHR cycle	Heat source	Working fluid	Expander	Sim.	Exp.	Mounted?	Coupling	Contribution	Tests	Ref.
1983	Thermo Electron	Mack 676 DE	215	ORC	Exhaust	Fluorinol-50	Axial turbine	√	√	√	Mechanical	12.5%[r]	2000-h on-road	[12, 13]
2012	Bosch	12L DE	n.a.[*]	RC/ ORC	Exhaust, EGR	Water/ Ethanol	Piston expander/ Turbine	√	√	×	Mechanical/ Electrical	4%-5%[r]	ESC	[14]
2012	Behr Thermal Systems	12L DE	300	ORC	Exhaust, EGR	Ethanol	Piston expander	√	√	×	n.a.	2%-6%[r]	ESC	[15]
2014	Hino Motors	n.a.	n.a.	ORC	EGR, Coolant, (Exhaust)	Hydro-fluoro-ether	Turbine	√	√	×	n.a.	3.8%[r] (7.5%[r])	Specific heat sources	[16]
2014	Cummins	Cummins ISX DE	350	ORC	Exhaust, EGR	R245fa	Turbine	√	√	√	Mechanical	3.6%[a]	500-miles on-road	[17, 18]
2015	Daimler	Detroit Diesel DD15	350	ORC	Exhaust, (EGR)	Ethanol	Scroll expander	√	×	×	Electrical	1.3%[a] (2.3%[a])	×	[19]
2016	Volvo	Volvo D13	360	RC	Exhaust	Water	Axial turbine	√	√	√	Mechanical	2%[a]	n.a.	[18, 20]
2017	Eaton	PACCAR MX13	360	ORC	Exhaust, EGR, Coolant, CAC, Oil cooler	Engine coolant	Roots expander	√	×	×	n.a.	3%-5%[a]	ESC	[21]

[*] n.a.: not available.

[a] Absolute improvement in engine efficiency or fuel economy.

[r] Relative improvement in engine efficiency or fuel economy.

Appendix B

Detailed data for calibration of the ICE model, used in Figure 3.

Table B.1. Experimental data for ICE calibration.

N_{ICE} (rpm)	bsfc (g/kWh)	W_{ICE} (kW)	T_{ICE} (N.m)	m_{air} (kg/s)	m_{exh} (kg/s)	$P_{IC,in}$ (kPa)	$P_{IC,out}$ (kPa)	$T_{IC,out}$ (ºC)	T_{exh} (ºC)
1200	196.1	156.9	1250.0	0.186	0.195	220.3	220.3	59.8	592.4
1400	191.8	186.2	1272.2	0.244	0.254	251.1	250.7	63.1	566.5
1600	196.3	213.8	1280.0	0.290	0.302	268.3	268.1	66.2	580.9
1800	202.2	240.2	1279.8	0.329	0.343	276.4	275.9	69.0	611.1
2000	206.4	242.0	1161.6	0.357	0.370	272.9	272.0	69.4	588.7
2200	214.2	240.6	1048.2	0.388	0.402	271.7	271.3	70.9	584.7

Table B.2. Simulation results of detailed model for ICE calibration.

N_{ICE} (rpm)	bsfc (g/kWh)	W_{ICE} (kW)	T_{ICE} (N.m)	m_{air} (kg/s)	m_{exh} (kg/s)	$P_{IC,in}$ (kPa)	$P_{IC,out}$ (kPa)	$T_{IC,out}$ (ºC)	T_{exh} (ºC)
1200	206.3	148.8	1183.9	0.162	0.171	204.2	202.7	59.6	646.6
1400	198.5	179.9	1227.0	0.229	0.239	249.8	247.0	62.8	582.4
1600	195.8	214.0	1277.0	0.277	0.289	267.8	264.0	65.8	568.8
1800	199.0	244.2	1295.7	0.317	0.331	275.6	270.9	68.5	582.4
2000	223.0	224.2	1070.5	0.345	0.359	272.6	267.0	68.9	616.0
2200	234.6	220.0	954.9	0.371	0.385	271.6	265.2	70.3	623.3

Table B.3. Simulation results of fast running model (FRM) for ICE calibration.

N_{ICE} (rpm)	bsfc (g/kWh)	W_{ICE} (kW)	T_{ICE} (N.m)	m_{air} (kg/s)	m_{exh} (kg/s)	$P_{IC,in}$ (kPa)	$P_{IC,out}$ (kPa)	$T_{IC,out}$ (ºC)	T_{exh} (ºC)
1200	202.4	151.7	1207.3	0.171	0.180	210.7	208.8	59.7	646.8
1400	195.5	182.6	1245.3	0.233	0.242	249.7	246.3	62.8	603.3
1600	192.4	217.7	1299.5	0.283	0.295	268.1	263.8	65.5	558.5
1800	195.5	248.7	1319.1	0.321	0.335	276.2	270.8	68.1	580.3
2000	218.3	229.1	1093.8	0.347	0.361	273.1	266.8	68.5	618.8
2200	229.6	224.8	975.7	0.372	0.386	272.2	264.8	70.1	631.3

References

[1] Lion S, Michos CN, Vlaskos I, Rouaud C, Taccani R. A review of waste heat recovery and organic Rankine cycles (ORC) in on-off highway vehicle heavy duty diesel engine applications. Renewable and Sustainable Energy Reviews 2017; 79:691-708.

[2] Hoang AT. Waste heat recovery from diesel engines based on Organic Rankine Cycle. Applied Energy 2018; 231:138-66.

[3] Xu B, Rathod D, Kulkarni S, Yebi A, Filipi Z, Onori S, Hoffman M. Transient dynamic modeling and validation of an organic Rankine cycle waste heat recovery system for heavy duty diesel engine applications. Applied Energy 2017; 205:260-79.

[4] Chatzopoulou MA, Markides CN. Thermodynamic optimisation of a high-electrical efficiency integrated internal combustion engine-Organic Rankine cycle combined heat and power system. Applied Energy 2018; 226:1229-51.

[5] Agudelo AF, García-Contreras R, Agudelo JR, Armas O. Potential for exhaust gas energy recovery in a diesel passenger car under European driving cycle. Applied Energy 2016; 174:201-12.

[6] Chatzopoulou MA, Simpson M, Sapin P, Markides CN. Off-design optimisation of organic Rankine cycle (ORC) engines with piston expanders for medium-scale combined heat and power applications. Applied Energy 2019; 238:1211-36.

[7] Shu G, Li X, Tian H, Shi L, Wang X, Yu G. Design condition and operating strategy analysis of CO_2 transcritical waste heat recovery system for engine with variable operating conditions. Energy Conversion and Management 2017; 142:188-99.

[8] Zhao R, Zhang H, Song S, Tian Y, Yang Y, Liu Y. Integrated simulation and control strategy of the diesel engine-organic Rankine cycle (ORC) combined system. Energy Conversion and Management 2018; 156:639-54.

[9] Usman M, Imran M, Yang Y, Park BS. Impact of organic Rankine cycle system installation on light duty vehicle considering both positive and negative aspects. Energy Conversion and Management 2016; 112:382-94.

[10] Xie H, Yang C. Dynamic behavior of Rankine cycle system for waste heat recovery of heavy duty diesel engines under driving cycle. Applied Energy 2013; 112:130-41.

[11] Battista DD, Mauriello M, Cipollone R. Waste heat recovery of an ORC-based power unit in a turbocharged diesel engine propelling a light duty vehicle. Applied Energy 2015; 152:109-20.

[12] Patel PS, Doyle EF. Compounding the truck diesel engine with an organic Rankine-cycle system. SAE Technical Paper 760343, 1976. https://doi.org/10.4271/760343.

[13] DiBella FA, DiNanno LR, Koplow MD. Laboratory and on-highway testing of diesel organic Rankine compound long-haul vehicle engine. SAE Technical Paper 830122, 1983. https://doi.org/10.4271/830122.

[14] Seher D, Lengenfelder T, Gerhardt J, Eisenmenger N, Hackner M, Krinn I. Waste heat recovery for commercial vehicles with a rankine process. 21st Aachen Colloquium Automobile and Engine

Technology 2012. https://www.aachener-kolloquium.de/images/tagungsunterlagen/2012_21._ACK/E3.3_Seher_Bosch.pdf.

[15] Edwards S, Eitel J, Pantow E, Geskes P, Lutz R. Waste heat recovery: the next challenge for commercial vehicle thermomanagement. SAE Int J Commer Veh 2012; 5(1):395-406.

[16] Furukawa T, Masaaki N, Machida K, Shimokawa K. A study of the Rankine cycle generating system for heavy duty hv trucks. SAE Technical Paper 2014-01-0678. https://doi.org/10.4271/2014-01-0678.

[17] Koeberlein D. Cummins supertruck program - technology and system level demonstration of highly efficient and clean, diesel powered class 8 trucks. 2015 Annual Merit Review, June 12. https://energy.gov/sites/prod/files/2015/06/f23/ace057_koeberlein_2015_o.pdf.

[18] Delgado O, Lutsey N. The U.S. supertruck program-expediting the development of advanced heavy-duty vehicle efficiency technologies. USA: International council on clean transportation: 2014.

[19] Singh S. Recovery act-class 8 truck freight efficiency improvement project. 2015 Annual Merit Review. https://energy.gov/sites/prod/files/2015/06/f23/ace058_singh_2015_o.pdf.

[20] Gibble J. Powertrain technologies for efficiency improvement. 2016 Annual Merit Review. https://energy.gov/sites/prod/files/2016/06/f32/ace060_amar_2016_o_web.pdf.

[21] Subramanian S. Affordable Rankine cycle (ARC) waste heat recovery for heavy duty trucks. 2017. https://www.energy.gov/sites/prod/files/2017/06/f34/acs097_subramanian_2017_o.pdf.

[22] Zhang H, Wang E, Fan B. A performance analysis of a novel system of a dual loop bottoming organic Rankine cycle (ORC) with a light-duty diesel engine. Applied Energy 2013; 102:1504-13.

[23] Preißinger M, Schwöbel JA, Klamt A, Brüggemann D. Multi-criteria evaluation of several million working fluids for waste heat recovery by means of organic Rankine cycle in passenger cars and heavy-duty trucks. Applied Energy 2017; 206(Supplement C):887-99.

[24] Shu G, Zhao M, Tian H, Wei H, Liang X, Huo Y, Zhu W. Experimental investigation on thermal OS/ORC (oil storage/organic Rankine cycle) system for waste heat recovery from diesel engine. Energy 2016; 107:693-706.

[25] Chen Y, Lundqvist P, Platell P. Theoretical research of carbon dioxide power cycle application in automobile industry to reduce vehicle's fuel consumption. Applied Thermal Engineering 2005; 25(14-15):2041-53.

[26] Chen Y, Lundqvist P, Johansson A, Platell P. A comparative study of the carbon dioxide transcritical power cycle compared with an organic rankine cycle with R123 as working fluid in waste heat recovery. Applied Thermal Engineering 2006; 26(17-18):2142-7.

[27] Sarkar J. Review and future trends of supercritical CO_2 Rankine cycle for low-grade heat conversion. Renewable and Sustainable Energy Reviews 2015; 48:434-51.

[28] Santini L, Accornero C, Cioncolini A. On the adoption of carbon dioxide thermodynamic cycles for nuclear power conversion: A case study applied to Mochovce 3 Nuclear Power Plant. Applied Energy 2016; 181:446-63.

[29] Persichilli M, Kacludis A, Zdankiewicz E, Held T. Supercritical CO_2 power cycle developments and commercialization: why sCO_2 can displace steam. Power-Gen India & Central Asia, New Delhi, India.

[30] Shu G, Shi L, Tian H, Li X, Huang G, Chang L. An improved CO_2-based transcritical Rankine cycle (CTRC) used for engine waste heat recovery. Applied Energy 2016; 176:171-82.

[31] Shi L, Shu G, Tian H, Huang G, Chang L, Chen T, Li X. Ideal point design and operation of CO_2-based transcritical Rankine cycle (CTRC) system based on high utilization of engine's waste heats. Energies 2017; 10(11):1692.

[32] Farzaneh-Gord M, Mirmohammadi SA, Behi M, Yahyaie A. Heat recovery from a natural gas powered internal combustion engine by CO_2 transcritical power cycle. Thermal Science 2010; 14(4):897-911.

[33] Shu G, Shi L, Tian H, Deng S, Li X, Chang L. Configurations selection maps of CO_2-based transcritical Rankine cycle (CTRC) for thermal energy management of engine waste heat. Applied Energy 2017; 186(3):423-35.

[34] Wu C, Yan X, Wang S, Bai K, Di J, Cheng S, Li J. System optimisation and performance analysis of CO_2 transcritical power cycle for waste heat recovery. Energy 2016; 100:391-400.

[35] Li X, Shu G, Tian H, Shi L, Wang X. Dynamic modeling of CO_2 transcritical power cycle for waste heat recovery of gasoline engines. Energy Procedia 2017; 105:1576-81.

[36] Farouk B, Hasan N. Transcritical carbon dioxide flow in a tubular heat exchanger: applications in waste heat recovery. Computational Themal Sciences 2016; 8(4):321-36.

[37] Wang Y, Shu G, Yu G, Tian H, Ma X, Chen T. Numerical analysis of forced convection of high-temperature exhaust gas around a metal-foam wrapped cylinder. International Journal of Heat and Mass Transfer 2018; 119:742-51.

[38] Qi J, Reddell T, Qin K, Hooman K, Jahn I . Supercritical CO_2 radial turbine design performance as a function of turbine size parameters. Journal of Turbomachinery 2017; 139(8):081008-11.

[39] Shi L, Shu G, Tian H, Huang G, Chen T, Li X, Li D. Experimental comparison between four CO_2-based transcritical Rankine cycle (CTRC) systems for engine waste heat recovery. Energy Conversion and Management 2017; 150:159-71.

[40] Li X, Shu G, Tian H, Shi L, Huang G, Chen T, Liu P. Preliminary tests on dynamic characteristics of a CO_2 transcritical power cycle using an expansion valve in engine waste heat recovery. Energy 2017; 140:696-707.

[41] Li X, Shu G, Tian H, Huang G, Liu P, Wang X, Shi L. Experimental comparison of dynamic responses of CO_2 transcritical power cycle systems used for engine waste heat recovery. Energy Conversion and Management 2018; 161:254-65.

[42] Li X, Tian H, Shu G, Hu C, Sun R, Li L. Effects of external perturbations on dynamic performance of carbon dioxide transcritical power cycles for truck engine waste heat recovery. Energy 2018; 163:920-31.

[43] Ge Y, Li L, Luo X, Tassou SA. Performance evaluation of a low-grade power generation system with CO_2 transcritical power cycles. Applied Energy 2017; 227:220-30.

[44] Pan L, Li B, Wei X, Li T. Experimental investigation on the CO_2 transcritical power cycle. Energy 2016; 95:247-54.

[45] Shu G, Zhao M, Tian H, Huo Y, Zhu W. Experimental comparison of R123 and R245fa as working fluids for waste heat recovery from heavy-duty diesel engine. Energy 2016; 115:756-769.

[46] Yu G, Shu G, Tian H, Huo Y, Zhu W. Experimental investigations on a cascaded steam-/organic-Rankine-cycle (RC/ORC) system for waste heat recovery (WHR) from diesel engine. Energy Conversion and Management 2016; 129:43-51.

[47] Shi L, Tian H, Shu G, Wei H, Liang X, Wang Y, Li X. An adjustable exhaust gas heat exchanger using carbon dioxide. China patent ZL201720224886.7, 2017-05-24. (in Chinese).

[48] Kuppan T. Heat exchanger design handbook, Second Edition. CRC Press, 2013.

[49] Yan Y, Lio H, Lin T. Condensation heat transfer and pressure drop of refrigerant R-134a in a plate heat exchanger. International Journal of Heat and Mass Transfer, 1999; 42:993-1006.

[50] Aakenes F. Frictional pressure-drop models for steady-state and transient two-phase flow of carbon dioxide. Norwegian University of Science and Technology, 2012.

[51] Gamma Technologies. GT-SUITE flow theory manual, 2016.